ZDHHC3 Tyrosine Phosphorylation Regulates Neural Cell Adhesion Molecule Palmitoylation

Patricia Marie-Jeanne Lievens,[a,b] Tatiana Kuznetsova,[a,c] Gaga Kochlamazashvili,[a] Fabrizia Cesca,[a] Natalya Gorinski,[d] Dalia Abdel Galil,[d] Volodimir Cherkas,[d] Natalia Ronkina,[e] Juri Lafera,[e] Matthias Gaestel,[e] Evgeni Ponimaskin,[d] Alexander Dityatev[a,f,g,h]

Department of Neuroscience and Brain Technologies, Istituto Italiano di Tecnologia, Genoa, Italy[a]; Department of Neurosciences, Biomedicine and Movement Sciences, Section of Biology and Genetics, University of Verona, Verona, Italy[b]; St. Petersburg State University, St. Petersburg, Russia[c]; Department of Cellular Neurophysiology, Hannover Medical School, Hannover, Germany[d]; Department of Physiological Chemistry, Hannover Medical School, Hannover, Germany[e]; Molecular Neuroplasticity Group, DZNE, Magdeburg, Germany[f]; Medical Faculty, Otto von Guericke University, Magdeburg, Germany[g]; Center for Behavioral Brain Sciences (CBBS), Magdeburg, Germany[h]

The neural cell adhesion molecule (NCAM) mediates cell-cell and cell-matrix adhesion. It is broadly expressed in the nervous system and regulates neurite outgrowth, synaptogenesis, and synaptic plasticity. Previous *in vitro* studies revealed that palmitoylation of NCAM is required for fibroblast growth factor 2 (FGF2)-stimulated neurite outgrowth and identified the zinc finger DHHC (Asp-His-His-Cys)-containing proteins ZDHHC3 and ZDHHC7 as specific NCAM-palmitoylating enzymes. Here, we verified that FGF2 controlled NCAM palmitoylation *in vivo* and investigated molecular mechanisms regulating NCAM palmitoylation by ZDHHC3. Experiments with overexpression and pharmacological inhibition of FGF receptor (FGFR) and Src revealed that these kinases control tyrosine phosphorylation of ZDHHC3 and that ZDHHC3 is phosphorylated by endogenously expressed FGFR and Src proteins. By site-directed mutagenesis, we found that Tyr18 is an FGFR1-specific ZDHHC3 phosphorylation site, while Tyr295 and Tyr297 are specifically phosphorylated by Src kinase in cell-based and cell-free assays. Abrogation of tyrosine phosphorylation increased ZDHHC3 autopalmitoylation, enhanced interaction with NCAM, and upregulated NCAM palmitoylation. Expression of ZDHHC3 with tyrosine mutated in cultured hippocampal neurons promoted neurite outgrowth. Our findings for the first time highlight that FGFR- and Src-mediated tyrosine phosphorylation of ZDHHC3 modulates ZDHHC3 enzymatic activity and plays a role in neuronal morphogenesis.

Protein *S*-palmitoylation is attachment of a 16-carbon fatty acid to a cysteine residue(s) via a thioester linkage. The reaction is catalyzed by protein acyltransferases (PATs), while the removal of fatty acids from proteins is controlled by specific thioesterases. Twenty-three members of the PAT family containing a conserved Asp-His-His-Cys (DHHC) signature motif (1–5) and three thioesterases, APT1, APT2 (6), and APT1-like (7), have been identified to date. The reversibility of palmitoylation confers on this modification the property to regulate stability, intracellular trafficking, functional activity, and interactions of the proteins, as exemplified by the studies on the Ras family of small GTPases (8, 9). Of particular interest is the role of palmitoylation in neuronal development and synaptic plasticity, where it regulates precise trafficking and distribution of proteins to specialized compartments on the pre- and postsynaptic sides, including proteins that mediate neurotransmitter synthesis and release, synaptic vesicle proteins, neurotransmitter receptors, postsynaptic scaffolds, and various signaling proteins (10). Palmitoylation of transmembrane proteins often induces their association with lipid rafts (11), where many signaling, adhesion, and cytoskeletal molecules are assembled, including those critical for neurite outgrowth (12–15).

One of the palmitoylated neural proteins is a cell adhesion molecule, neural cell adhesion molecule (NCAM), that plays a key role in neurite outgrowth, synaptogenesis, and synaptic plasticity (16, 17). Three cysteines located in the juxtamembrane portion of transmembrane NCAM isoforms (NCAM140 and NCAM180) have been identified as acylation sites (5), where palmitate is the predominant lipid (18). Several studies revealed that NCAM-mediated neurite outgrowth requires NCAM palmitoylation and translocation to the lipid rafts, where upon the recruitment of Fyn and Fak kinases, it engenders a signaling cascade leading to neurite elongation (19, 20). For some signaling cascades known to be stimulated downstream of NCAM, for instance, the one leading to extracellular signal-regulated kinase (ERK) phosphorylation, activation of the fibroblast growth factor (FGF) receptor (FGFR) is also required (19, 21, 22). Reciprocally, it was shown that FGF2 application and FGFR signaling stimulate NCAM palmitoylation in both neuroblastoma cells and primary hippocampal neurons (18), promoting NCAM raft translocation. Screening of the 23 mammalian PATs (also referred to as ZDHHCs) led to the identification of ZDHHC3 and ZDHHC7 as the two closely related enzymes showing the highest palmitoylating activity toward

Accepted 17 May 2016

Citation Lievens PM-J, Kuznetsova T, Kochlamazashvili G, Cesca F, Gorinski N, Galil DA, Cherkas V, Ronkina N, Lafera J, Gaestel M, Ponimaskin E, Dityatev A. 2016. ZDHHC3 tyrosine phosphorylation regulates neural cell adhesion molecule palmitoylation.

Address correspondence to Evgeni Ponimaskin, ponimaskin.evgeni@mh-hannover.de, or Alexander Dityatev, alexander.dityatev@dzne.de.

P.M.-J.L. and T.K. contributed equally to the study.

Supplemental material for this article may be found **online**

NCAM. In light of these data, it is plausible to expect FGFR signaling to regulate ZDHHC3 and ZDHHC7 functions (18). In the present study, we focused on the molecular mechanisms regulating activity of ZDHHC3, which represents a more extensively characterized ZDHHC family member with a proven key regulatory role in controlling synaptic functions in the central nervous system (10, 23, 24).

ZDHHC3, also known as GODZ (Golgi apparatus-specific DHHC zinc finger protein), has been shown to palmitoylate AMPA (25), NMDA (26–28), and $GABA_A$ (29) receptors and hence to control their trafficking at the synapses. In addition, ZDHHC3 can palmitoylate a number of proteins involved in control of neuronal morphogenesis, such as the α6 integrin subunit (30), Gαs and Gαq proteins (31–33), and stathmins 2 and 3 (34). Despite the long list of substrates (10), little is known regarding the molecular mechanisms regulating the enzymatic activity of ZDHHC3. Recently, Jennings and Linder (35) proved that ZDHHC3 utilizes a "ping-pong" kinetic mechanism to transfer palmitate to the target protein, while no regulatory sites on the ZDHHC3 protein have yet been discovered. In the present study, we identified ZDHHC3 tyrosine residues as specific targets for FGFR1 and Src kinases and showed that their replacement results in increased ZDHHC3 autopalmitoylation levels and upregulation of NCAM180 palmitoylation. We also validated the physiological relevance of tyrosines by a morphological assay, which revealed an increase in the total neurite length of cultured hippocampal neurons expressing the tyrosine-mutated ZDHHC3. In addition, we report on tyrosine phosphorylation of endogenously expressed ZDHHC3 in the brain and demonstrate FGF2-mediated increase of NCAM palmitoylation *in vivo*.

MATERIALS AND METHODS

Antibodies. Rabbit polyclonal anti-ZDHHC3 ab31837 was from Abcam, rabbit polyclonal anti-Src (sc-18) from Santa Cruz, mouse monoclonal anti-Src from Cell Signaling (L4A1), mouse monoclonal anti-NCAM clone OB-11 from Sigma (C9672), rabbit monoclonal anti-GM130 (clone EP892Y) from Abcam (ab52649), mouse monoclonal antipolyhistidine clone His-1 from Sigma (H1029), rabbit phospho-FGFR (Tyr653/654) from Cell Signaling (3471), mouse monoclonal anti-β-tubulin from Sigma (T5201), rabbit anti-β-tubulin III from Sigma-Aldrich (T2200), rabbit polyclonal anticalnexin from Enzo Life Sciences (ADI-SPA-860), mouse monoclonal antihemagglutinin (anti-HA) clone 12CA5 from Roche (11583816001), polyclonal rabbit anti-HA Y-11 from Santa Cruz (sc-805), and rabbit polyclonal anti-GABAγ2 subunit (224003) and rabbit polyclonal anti-PSD95 (124002) from Synaptic Systems. Goat anti-mouse (PR31430) and goat anti-rabbit (PR31460) horseradish peroxidase (HRP)-conjugated antibodies were from Thermo Scientific Pierce, and Alexa Fluor 568 and 633 goat anti-rabbit IgGs were from Invitrogen (A11036 and A21071, respectively).

Chemicals from regular commercial sources used in the study. Protein G-Sepharose (17-0618-01), streptavidin-Sepharose (17-5113-01), ECL plus (RPN 2133) or ECL prime Western blotting (WB) detection reagent (RPN2232), and Hyperfilm ECL (GEH28906837) were from GE Healthcare. Page ruler prestained protein ladder plus (PR26620), nonfat dried milk powder (EMR180001), and Westran CS 0.45-μm polyvinylidene difluoride (PVDF) blotting membranes (10485289) were purchased from Euroclone. The DC protein assay kit (500-0111) was from Bio-Rad. Phosphatase inhibitor cocktail 2 for tyrosine protein phosphatases, acid and alkaline (P5726), and phosphatase inhibitor cocktail 3 for serine/threonine protein phosphatases and L-isozymes of alkaline phosphatase (P0044), aprotinin from bovine lung (A1153), Pefabloc (76307), and leupeptin (L2884) were from Sigma. The solvents dimethyl sulfoxide (DMSO) and dimethylformamide (DMF) (D4551) were from Sigma-Aldrich.

The selective Src inhibitor PP2 {4-amino-5-(4-chlorophenyl)-7-(*t*-butyl)pyrazolo[3,4-D]-pyrimidine} (529573) and its negative control, PP3 (4-amino-7-phenylpyrazolo[3,4-D]pyrimidine) (529574), were from Calbiochem, and the inhibitor of FGFR autophosphorylation PD 173074 was from Sigma (P2499). All the inhibitors were dissolved in DMSO to 1,000× stock. Palmitic acid-azide was dissolved in DMSO to 1,000× stock (50 mM), and biotin-alkyne was dissolved in DMF to 100× stock (4 mM).

Dulbecco's modified Eagle's medium (DMEM) (41965062), Opti-MEM 1 (31985047), fetal bovine serum (FBS) (10270106), penicillin-streptomycin (PenStrep; 15140122), sodium pyruvate (11360039), trypsin 0.25% EDTA (25200056), phosphate-buffered saline (PBS) (10010056), neurobasal medium (21103049), basal medium Eagle (BME) (41010-026), B27 supplement (17504044), and GlutaMax 1 (35050038) were purchased from Life Technologies; 45% D-(+)-glucose solution (G8769), poly-D-lysine (PDL) hydrobromide (P6407), and poly-L-lysine (PLL) hydrobromide (P2636) were from Sigma.

Lipofectamine 2000 reagent (11668) was from Invitrogen, and X-tremeGene 9 DNA transfection reagent (06365787001) was from Roche; Amaxa P3 primary culture 4D-nucleofector 32 RCT (V4XP-3032) was from Lonza. Vectashield mounting medium with DAPI (4′,6-diamidino-2-phenylindole) was from Vector Laboratories (H-1200).

Recombinant cDNA procedures. ZDHHC7 cDNA was subcloned into pEF-Bos-HA and mouse ZDHHC3 into pEF-Bos-HA or pEGFP (enhanced green fluorescent protein)-C1 (kindly provided by M. Fukata); rat NCAM180 in the pcDNA3 vector was described previously (19). Human FGFR1 was subcloned into pCMV-His (kindly provided by I. Tomoko, University of Glasgow). pCMV5 mouse Src was a gift from Joan Brugge and Peter Howley (Addgene plasmid 13663). 3× HA and EGFP tags were at the N terminus of the ZDHHC3 protein, and the His tag was located at the C terminus of the FGFR1 protein. An NCAM180Δ construct, in which the four cysteine residues located in the intracellular domain adjacent to transmembrane domain were replaced by serines, and an HA-ZDHHC3/C157S construct abolishing the catalytic activity of the enzyme were described previously (19, 34, 36, 37). A plasmid encoding the γ2 subunit of the GABA receptor was kindly provided by Andrea Barberis.

Mouse ZDHHC3 and ZDHHC3-C175S cDNAs were subcloned into pcDNA3.0 (Invitrogen) to generate their untagged versions. Plasmids encoding ZDHHC3 mutants with single- and triple-tyrosine (Y) replacements by phenylalanine (F) were generated with the QuikChange site-directed mutagenesis kit according to the manufacturer's instructions (Stratagene) using the primers listed in Table 1. The same kit was used to generate catalytically inactive ZDHHC3 mutants by replacing cysteine (C157) with serine (S). The primers used for mutagenesis are summarized in Table 1. The new molecules were verified by sequencing. The green fluorescent protein (GFP)–ZDHHC3/Y18F-Y127F-Y171F-Y295F-Y297F construct was generated by subcloning the corresponding untagged ZDHHC3 mutant into the EGFP-C1 vector.

Cell cultures. Neuroblastoma N2a cells (CCL-131) and mouse cells deficient in Src, Yes, and Fyn ($SYF^{-/-}$ cells) (CRL 2459) were purchased from ATCC. They were grown in DMEM containing 10% FBS, 1% penicillin-streptomycin, and 1% sodium pyruvate at 37°C under 5% CO_2. For transient transfection, cells were seeded at low density 12 h before transfection. N2a and $SYF^{-/-}$ cells were transiently transfected with appropriate vectors according to the manufacturer's instructions using Lipofectamine 2000 or X-tremeGene 9, as indicated. In some experiments, N2a cells were treated 24 h after transfection with 5 μM PD173074, 10 μM PP2, or 10 μM PP3 for 2 h.

Assessment of ZDHHC3 tyrosine phosphorylation. Cell lysates and immunoprecipitations were performed as previously described (38), with some modifications. Twenty-four hours after transfection, N2a cells were washed with ice-cold PBS supplemented with 1 mM Na_3VO_4 and 50 mM NaF to preserve the protein phosphorylation states and lysed in RIPA buffer (150 mM NaCl, 1% NP-40, 0.5% sodium deoxycholate, 0.1% SDS, 50 mM Tris, pH 8) containing aprotinin (3 μg/ml), leupeptin (1 μg/ml),

TABLE 1 Primers used for site-directed mutagenesis of ZDHHC3

ZDHHC3 mutant	Primer	Oligonucleotide sequence[a] (5′→3′)
Y18F	For	AGCGGAAACCAGAGT**T**CCTCCAGCCAGAG
	Rev	CTCTGGCTGGAGG**A**ACTCTGGTTTCCGCT
Y127F	For	TGGGCAGGTGGTGT**T**CAAGTGTCCCAAGTG
	Rev	CACTTGGGACACTTG**A**ACACCACCTGCCCA
Y171F	For	GAGAACAACCAGAAGT**T**CTTTGTCCTATTCACA
	Rev	TGTGAATAGGACAAAGAACTTCTGGTTGTTCTC
Y295F/Y297F	For	AAGGCAGACCCGT**T**CCAGT**T**TGTGGTCTGAGG
	Rev	CCTCAGACCACA**A**ACTGG**A**ACGGGTCTGCCTT
C157S	For	GCAAGATGGATCACCAC**A**GTCCTTGGGTCAACAA
	Rev	TTGTTGACCCAAGGAC**T**GTGGTGATCCATCTTGC
P27A/P30A	For	AGAGAAGTGTGCCCCA**G**CTCCCTTC**G**CTGGTCCTGCGGGA
	Rev	TCCCGCAGGACCAG**C**GAAGGGAG**C**TGGGGCACACTTCTCT

[a] Boldface, mutated nucleotides.

pepstatin (1 μg/ml), Pefabloc (0.2 mM), EDTA (2.5 mM), Na fluoride (50 mM), and phosphatase inhibitor cocktails 2 and 3 (1% each). After 20-min incubation on ice, the lysates were centrifuged for 10 min at 20,000 × *g*, and the supernatants were collected.

Immediately after lysis, HA-tagged or untagged ZDHHC3 was immunoprecipitated from 1,000 μg of the lysates using anti-HA or anti-ZDHHC3 (anti-GODZ), respectively. Immune complexes were released from protein G-Sepharose beads by incubation for 10 min at 100°C in reducing electrophoresis sample buffer (SB) (4% SDS, 20% glycerol, 120 mM Tris, 0.01% bromophenol blue, pH 7.8, 0.2 M dithiothreitol [DTT], 4% β-mercaptoethanol [BME]) and separated by SDS-PAGE on 12% acrylamide gels. After transfer to PVDF membranes, they were first incubated with phosphoblocker (5% bovine serum albumin [BSA], 1% PVP-10, 1% polyethylene glycol [PEG] 3500, 0.2% Tween 20, 2× PBS) and then probed with 4G10 antibody (1:5,000 in 5% BSA–Tris-buffered saline with 0.2% Tween 20 [TBST]) to evaluate tyrosine phosphorylation of ZDHHC3/7. The total amount of HA-tagged ZDHHC3/7 or untagged ZDHHC3 was analyzed on the same PVDF membrane after stripping by immunoblotting (IB) with anti-HA or anti-ZDHHC3 antibody, respectively. The phosphorylation levels of different ZDHHC3 mutants or of ZDHHC3 after different treatments were measured. The protein expression level of transfected constructs was documented in extracts by IB of these molecules. In parallel, the expression of the tubulin housekeeping gene was determined.

Co-IP experiments. Interaction between ZDHHC3 and NCAM180 or the γ2 subunit of the GABA receptor in N2a cells or Src kinase in SYF$^{-/-}$ cells was analyzed by coimmunoprecipitation (co-IP) as described elsewhere (36, 39). Interaction between NCAM180 and ZDHHC3 was estimated in N2a cells cotransfected with NCAM180 and untagged wild-type (wt) ZDHHC3 (ZDHHC3wt) or mutant ZDHHC3 (Y18F-Y127F-Y171F-Y295F-Y297F, Y127F-Y171F-Y295F-Y297F, Y18F-Y127F-Y171F, and C157S). ZDHHC3 was enriched by IP (as described above) from N2a cells lysed in RIPA buffer. Precipitated proteins from immune complexes were separated by SDS-PAGE on 12% acrylamide gels (see Fig. 6) and transferred to PVDF membranes. To analyze the levels of immunoprecipitated ZDHHC3 and NCAM180 that were pulled down, the membranes were probed with anti-ZDHHC3 and anti-NCAM (lower and upper parts of the membrane, respectively) antibodies. The expression levels of exogenous NCAM180 and ZDHHC3 were monitored by IB of extracts.

Src-ZDHHC3 interaction was assessed in a similar manner in SYF$^{-/-}$ cell cotransfection with Src and ZDHHC3wt, ZDHHC3/Y18F-Y127F-Y171F-Y295F-Y297F, ZDHHC3/C157S, ZDHHC3/P27A-P30A, ZDHHC3/P27A-P30A-Y295F-Y297F, and ZDHHC3/P27A-P30A-Y18F-Y127F-Y171F-Y295F-Y297F. Interaction of the γ2 subunit of the GABA receptor with wt or Y18F-Y127F-Y171F-Y295F-Y297F ZDHHC3 transfected in N2a cells was estimated in a similar manner.

Protein bands were captured by chemiluminescent detection using ImageQuant LAS 4000 (GE Healthcare; 28-9558-10) or on Hyperfilm ECL with subsequent development with the Curix 60 processing machine (AGFA).

Palmitoylation assay with radioactive metabolic labeling. Palmitoylation of NCAM180 transfected in N2a cells was assessed by radioactive [^{3}H]palmitate metabolic labeling followed by fluorographic detection, as described previously (18). To monitor NCAM palmitoylation, N2a cells cotransfected with NCAM180 and ZDHHC3wt or mutated ZDHHC3 forms were first preincubated for 30 min in serum-free DMEM with fatty acid-free bovine serum albumin (5 mg/ml; Sigma-Aldrich). The cells were then labeled with 0.25 mCi/ml [^{3}H]palmitate (PerkinElmer) for 4 h in the preincubation medium. After lysis in RIPA buffer, NCAM180 from the cell extracts was immunoprecipitated with mouse anti-NCAM antibodies (at a 1:100 dilution), and the immune complexes were released from the beads by incubation in nonreducing SB (62.5 mM Tris-HCl, pH 6.8, containing 20% glycerol, 6% SDS, and 0.002% bromophenol blue). The radiolabeled polypeptides were analyzed by SDS-PAGE on 10% acrylamide gels under nonreducing conditions and visualized by fluorography using Kodak X-Omat AR film. Expression of NCAM180 was confirmed by IB with anti-NCAM antibodies.

Densitometric analysis of fluorograms was performed with Gel-Pro Analyzer version 3.1 software (Media Cybernetics). For every ZDHHC3 mutant, palmitoylation levels of NCAM180 were given, after normalization to the expression level, as a relative value in comparison to NCAM180 palmitoylation obtained by ZDHHC3wt, which was set to 100%.

Phosphorylation of endogenous ZDHHC3 from the mouse brain. For the immunoprecipitation of endogenous ZDHHC3, whole brains of 2- to 3-month-old male C57BL6J mice were used. The mice were injected subcutaneously (s.c.) with approximately 100 μl of 12.5-μg/ml FGF2 (Sigma) or an equal volume of vehicle, 0.1% BSA in PBS. After 2 h, the mice were euthanized by cervical dislocation. All animal treatments were approved by the Italian Committee on Animal Health and Care. The brains were extracted into preoxygenated ice-cold dissection artificial cerebrospinal fluid (ACSF) containing 2.5 mM KCl, 1.25 mM NaH_2PO_4, 24 mM $NaHCO_3$, 1.5 mM $MgSO_4$, 2 mM $CaCl_2$, 25 mM glucose, and 250 mM sucrose; briefly dried on filter paper; quick-frozen in liquid nitrogen; and stored at −80°C. Then, the brain tissue was homogenized in HEPES buffer (10 mM HEPES, pH 7.4, 5 mM EGTA, 1 mM EDTA, and 0.32 M sucrose) containing phenylmethylsulfonyl fluoride (PMSF) (1 mM; Carl

Roth); leupeptin, chymostatin, antipain, and pepstatin (0.25 μg/ml each; Carl Roth); and phosphatase inhibitor cocktails 2 and 3 (1% each; Sigma-Aldrich). The homogenate was centrifuged, and the pellet was dissolved in lysis buffer (150 mM NaCl, 50 mM Tris, 5 mM EDTA, pH 7.4) containing PMSF, leupeptin, chymostatin, antipain, pepstatin, and phosphatase inhibitor cocktails 2 and 3. From this lysate, 50 μl was set aside as an input sample. ZDHHC3 was immunoprecipitated from the samples by incubation with 10 μl anti-GODZ antibody (anti-ZDHHC3; Abcam) overnight at 4°C, followed by incubation with protein A-Sepharose (Sigma; P3391) for 2 h at 4°C. After washing with RIPA or lysis buffer containing PMSF, leupeptin, chymostatin, antipain, pepstatin, and phosphatase inhibitor cocktails 2 and 3, the immune complexes were released from the beads by incubation with 50 μl electrophoresis sample buffer (62.5 mM Tris, pH 6.8, 6% SDS, 20% glycerol, 0.1% bromophenol blue) at 50°C for 20 min and subjected to SDS-PAGE (12% acrylamide gels). The proteins were transferred to nitrocellulose blotting membranes (Amersham; Protran Premium) and probed either with antiphosphotyrosine antibody clone 4G10 (Millipore; 1:500 in 5% BSA-TBST) or anti-GODZ antibody (Abcam; 1:1,000 in 5% milk-TBST). For quantification, the input samples were probed with the same antibodies. All the membranes were detected with SuperSignal West Femto maximum sensitivity substrate (Thermo Fisher Scientific) on a Fusion SL advanced MP device (Peqlab).

Palmitoylation of endogenous NCAM using the ABE procedure. *In vivo* palmitoylation of NCAM140 and -180 was performed using acyl-biotin exchange (ABE), as previously described (40). In brief, freshly resected mouse brains without the cerebellum were frozen in liquid nitrogen and stored at −80°C before use. After homogenization in buffer containing 10 mM HEPES, 1 mM EDTA, 5 mM EGTA, 320 mM sucrose, 1 mM PMSF, and protease inhibitors (0.25 μg/ml antipain, 0.25 μg/ml chymostatin, 0.25 μg/ml leupeptin, 0.25 μg/ml pepstatin), free thiol groups were blocked with 10 mM *N*-ethylmaleimide (NEM). To cleave thioester-linked palmitoyl moieties, 0.5 M hydroxylamine was applied, followed by labeling of newly exposed free thiol groups with 0.75 mM HPDP-biotin (ThermoScientific). Finally, the biotinylated proteins were purified, using streptavidin-agarose affinity chromatography, and visualized by Western blotting using anti-NCAM antibody (18). Samples without hydroxylamine treatment were used as a control for nonspecific biotin binding.

Palmitoylation assay using click reaction. Autopalmitoylation of ZDHHC3 transfected in N2a cells was monitored by nonradioactive click chemistry, which is becoming an attractive alternative to the radioactive method (41–45). Here, we applied a Click-iT assay (ThermoFisher Scientific) according to the manufacturer's instructions with some modifications, followed by enrichment of the palmitoylated protein pool and detection of the proteins of interest (ZDHHC3 and calnexin) by IB (see Fig. S4 in the supplemental material). To assess the autopalmitoylation of different ZDHHC3 mutants, proteins were metabolically labeled for 4 h with 50 μM palmitic acid-azide 24 h after transfection. The cells were lysed in high-SDS lysis buffer (50 mM Tris, pH 8.0, 1% SDS) containing leupeptin (1 μg/ml), Pefabloc (0.2 mM), and EDTA (2.5 mM). After 20-min incubation on ice, the cell lysates were sonicated twice for 10 s each time to break the DNA, vortexed for 5 min in a cold room (4°C), and centrifuged for 10 min at 20,000 × *g*. The cleared supernatants were collected, and the click reaction was carried out following the protocol provided (http://tools.lifetechnologies.com/content/sfs/manuals/mp10276.pdf) with some modifications. Briefly, 200 μg (maximum, 50 μl) of lysates (brought to the same concentration) were reacted with 4 mM biotin-alkyne by Cu(I)-catalyzed azide-alkyne cycloaddition (CuAAC) using a Click-iT protein reaction buffer kit to target palmitic acid-azide of metabolically labeled proteins with biotin (see Fig. S4 in the supplemental material). After methanol-chloroform precipitation, the proteins were dissolved in 350 μl of RIPA buffer containing leupeptin, EDTA, and Pefabloc at the concentrations indicated above and solubilized by sonication three times for 10 s each time. After solubilization, the palmitoylated proteins were enriched with streptavidin-Sepharose beads from 250 μl of the obtained lysates and separated under reducing conditions by SDS-PAGE on 12% acrylamide gels. Palmitoylated ZDHHC3 was monitored by IB with anti-ZDHHC3 antibodies. The same membrane was probed with anticalnexin antibody (used as an internal positive control for the palmitoylation reaction). The total amount of ZDHHC3 or calnexin in the lysates obtained after the Click-iT reaction was evaluated by IB of 10 or 20 μl of extracts with specific antibodies.

***In vitro* kinase assay.** Recombinant active human glutathione *S*-transferase (GST)–Src was from Sigma (S1076). Radioactive [γ-^{33}P]ATP was from Hartmann Analytic (SRF301). ATP lithium salt was from Boehringer Mannheim GmbH. ZDHHC3 was immunoaffinity purified from N2a cells. After 4 washes with 1 ml RIPA buffer (20 mM Tris, pH 7.4, 150 mM NaCl, 10 mM EDTA, 10 mM iodoacetamide, 0.1% SDS, 1% Triton X-100, 1% deoxycholic acid) containing PMSF (1 mM; Carl Roth), leupeptin, chymostatin, antipain, pepstatin (2.5 μg/ml each; Carl Roth), and phosphatase inhibitor cocktails 2 and 3 (1% each; Sigma-Aldrich), the beads were additionally washed with 1 ml of kinase dilution buffer (5 mM MOPS [morpholinepropanesulfonic acid], pH 7.2, 2.5 mM glycerol 2-phosphate, 4 mM $MgCl_2$, 2.5 mM $MnCl_2$, 1 mM EGTA, 0.4 mM EDTA, 0.05 mM DTT, and 50 ng/μl BSA). The resulting beads with immobilized ZDHHC3 were used as a substrate in an *in vitro* kinase assay with 10 ng active GST-Src in kinase dilution buffer supplemented with 250 μM ATP and 1 μCi [γ-^{33}P]ATP. The kinase reaction was carried out in a 25-μl final volume at 30°C for 15 min. The reaction was stopped by adding 8 μl 4× Laemmli buffer (0.25 M Tris-HCl, pH 6.8, 4% [mass/vol] SDS, 4 mM EDTA, 0.25% [mass/vol] bromophenol blue, 20% β-mercaptoethanol, 40% glycerol), and samples were heated to 96°C for 5 min. The protein samples were separated on a 7.5 to 22.5% polyacrylamide gradient gel. Radioactivity incorporated into the substrates was quantified by phosphorimaging using a FLA9000 (Fuji).

Immunocytochemistry and confocal imaging. Subcellular localization of GFP-tagged ZDHHC3wt and ZDHHC3/Y18F-Y127F-Y171F-Y295F-Y297F transfected into N2a cells was analyzed by confocal imaging after immune staining against the Golgi apparatus marker GM130. Immunocytochemical labeling was performed as previously described (46) with some modifications.

A day before transfection, N2a cells were plated at low density (15,000 cells per well) on 12-mm sterile coverslips coated with PLL (0.1 mg/ml) in a 24-well plate. The cells were transfected with the indicated plasmids (with 0.2 μg of DNA in total) using X-tremeGene 9. Twenty-four hours later, the cells were washed gently with PBS and fixed with 4% formaldehyde in PBS for 20 min. After abundant washes, the cells were permeabilized with 0.1% Triton X-100 and blocked with 2% BSA for 20 min. Following blocking, the cells were incubated overnight at 4°C with anti-GM130 (1:100) antibodies resuspended in 5% goat serum-PBS. For visualization, Alexa Fluor 633 (1:200) was used. The cells were embedded in Vectashield mounting medium with DAPI, and the images were acquired on a Leica SP5 inverted microscope with a 63× oil objective. DAPI was excited by a 405-nm diode (for UV), GFP was excited with the 488-nm line of an argon laser, and Alexa Fluor 633 with a helium-neon 633-nm laser.

Neurite outgrowth. Neurite outgrowth was performed as described previously (47), with minor modifications.

Hippocampal neurons (for morphometric analysis) were prepared from Charles River (wt) embryonic day 18 (E18) rat embryos. Pregnant females were purchased from Charles River (Calco, Italy). All procedures involving animals and their care were carried out in accordance with the guidelines established by the European Community Council (directive 2010/63/EU of 22 September 2010) and were approved by the Italian Ministry of Health. The rats were maintained under standard laboratory conditions (12-h light/dark cycle, 21 ± 1°C, and 40 to 70% humidity), with food and water provided *ad libitum*.

Immediately after preparation, hippocampal neurons were transiently transfected before plating by electroporation using Amaxa P3 primary culture 4D-Nucleofector 32 RCT according to the manufacturer's instructions (http://bio.lonza.com/fileadmin/groups/marketing/Downloads/Protocols/Generated/Optimized_Protocol_318.pdf) with

minor modifications. Briefly, 250,000 cells per group after trypsin dissociation, as described above, were aliquoted into 15-ml tubes and centrifuged at 800 rpm for 5 min, and the cell pellet was mixed with 4D-Nucleofector solution (16.4 μl of Nucleofector solution and 3.6 μl of supplement) containing 0.6 μg of total DNA. Then, the cell mixture was transferred into Nucleocuvette vessels and electroporated using the EM 110 program (high-efficacy transfection for rat hippocampal neurons). All the cells were cotransfected with untagged ZDHHC3wt, ZDHHC3/Y18F-Y127F-Y171F-Y295F-Y297F, or pcDNA3.1 vector and EGFP expression vector. Immediately after electroporation, the cells were diluted in preequilibrated attachment BME medium supplemented with 10% FBS, 0.3% glucose, 1% sodium pyruvate, and 1% HEPES and plated at a low density of 40,000 cells per 18-mm coverslip coated with PDL (0.1 mg/ml) in a 12-well plate. Three hours after plating, 3/4 of the medium was replaced with fresh preequilibrated neurobasal medium supplemented with 0.6% glucose, 1% GlutaMax, 0.9% PenStrep, and 2.8% B27. Cultures were maintained at 37°C in a humidified incubator gassed with 5% CO_2.

On day *in vitro* 2 (DIV2), the cells were briefly washed with PBS and fixed with 4% formaldehyde in PBS. After blocking and permeabilization as described above, the cells were incubated with anti-β-tubulin III (1:200) for 1.5 h and then stained with Alexa Fluor 568-conjugated secondary antibody for 1 h. Images were acquired on an Olympus BX51 upright fluorescence microscope with a 20× air objective using Neurolucida software. From each coverslip, several images were acquired using a UV filter (excitation with a 355- to 375-nm band-pass filter; emission with a 400- to 480-nm band-pass filter) for DAPI nucleus visualization, a fluorescein isothiocyanate (FITC) (GFP) filter (excitation with a 457- to 507-nm band-pass filter; emission with a 490- to 570-nm band-pass filter) for cells transfected with EGFP, and a TRITC filter (excitation with a 520- to 560-nm band-pass filter; emission with a 540- to 640-nm band-pass filter) for β-tubulin III staining to visualize the neuronal protrusions. The channels were merged using ImageJ software, and images of β-tubulin III staining of transfected EGFP-positive neurons were used for measurements. The neuron protrusions, longer than the cell bodies, were traced using a NeuronJ plug-in. Cells dead before fixation, with a pycnotic or fragmented nucleus (identified by DAPI), and cells with damaged neurites were excluded from the morphometric analysis. The length of the longest neurite, the total length of the neurites, and the number of primary dendrites of a single neuron were analyzed. In total, there were 358, 347, and 270 cells analyzed for control (pcDNA3.1) and experimental ZDHHC3wt and ZDHHC3/Y18F-Y127F-Y171F-Y295F-Y297F groups, respectively. For each of 4 transfections, 2 coverslips per group were analyzed. For each coverslip, the mean values for the total length of neurites and length of the longest neurite (in micrometers) and the number of neurites were calculated; the mean values within a transfection for a certain group were calculated as an average between coverslips and then normalized to the control group, set to 100%.

Statistical analysis. For statistical evaluation of all experiments and the graphical representation of the data (except where indicated), SigmaPlot 11.0 software was used. The means and standard errors of the mean (SEM) were reported for each experimental group. The values in biochemical experiments were normalized beforehand to the control group within a single experiment. Since the control and experimental groups in a single experiment were from the same cell passage (in biochemical experiments) or from cells prepared from the same animal (in the case of hippocampal neurons used for morphometric analysis), we used repeated-measures (RM) or paired tests to determine statistical significance. To analyze Western blot data for FGF2-mediated ZDHHC3 phosphorylation in N2a cells, as well as the level of NCAM palmitoylation *in vivo*, normalization by the sum of the replicate method was applied (48). Statistical significance was determined by two-tailed unpaired Student's *t* test (for two groups) or by one-way RM analysis of variance (ANOVA) followed by Holm-Sidak comparison, or, if a normality distribution Shapiro-Wilk test failed, we used one-way ANOVA on ranks followed by Student-Newman-Keuls comparison. Differences were considered statistically significant at a P value of <0.05.

RESULTS

FGFR1 signaling induces ZDHHC3 tyrosine phosphorylation. We previously identified ZDHHC3 and ZDHHC7 as PATs for NCAM140 and -180 (18). This knowledge, together with the observation that FGF2 application affects NCAM palmitoylation, prompted us to investigate whether ZDHHC3 could be a direct target of FGFR signaling. Because FGFRs are tyrosine kinases, we hypothesized that ZDHHC3's enzymatic activity might be regulated by tyrosine phosphorylation. By *in silico* analysis of the amino acid sequence of ZDHHC3, we found five tyrosine residues facing the cytoplasm, two located upstream, and three downstream of the DHHC catalytic domain (Fig. 1A). To test for FGFR1-mediated ZDHHC3 phosphorylation, we cotransfected histidine-tagged FGFR1 with HA-tagged ZDHHC3 in N2a cells. No FGF2 was added, because transfected FGFR1 was activated through self-dimerization and subsequent autophosphorylation (49). Then, we immunoprecipitated ZDHHC3 with anti-HA antibody and performed IB with 4G10 antibody directed against phosphorylated tyrosines. Overexpression of FGFR1 induced strong tyrosine phosphorylation of recombinant ZDHHC3, readily detected on short-time exposures of the blots (Fig. 1B, right). Similar results were obtained with ZDHHC7, while no ZDHHC3/7 tyrosine phosphorylation was detected in the absence of FGFR1 under these conditions (Fig. 1B, left). However, on long-time exposures, we observed a mild but unequivocal tyrosine phosphorylation signal for ZDHHC3, suggesting that endogenous kinases could transfer phosphates to tyrosines present in ZDHHC3. To rule out the possibility that tyrosines of the triple-HA tag would contribute to the tyrosine phosphorylation signal, we excised it and repeated the experiment using anti-ZDHHC3 antibody. To estimate the phosphorylation level of enriched ZDHHC3, we calculated the ratio of the tyrosine phosphorylation signal (4G10) to the total protein level assessed by reincubation of the membrane with anti-ZDHHC3 antibodies after stripping. As shown in Fig. 1C, untagged ZDHHC3 (used in all subsequent experiments) also appeared to be tyrosine phosphorylated by endogenous kinases. Notably, in the presence of cotransfected FGFR1, untagged ZDHHC3 showed a remarkable increase in tyrosine phosphorylation (Fig. 1C) that was abolished by the FGFR1 blocker PD173074 (see Fig. S1 in the supplemental material). We then analyzed whether activation of endogenously expressed FGFR would enhance ZDHHC3 phosphorylation under conditions previously used to demonstrate that ZDHHC3 is a palmitoyltransferase responsible for NCAM palmitoylation (18). N2a cells transfected with the wild-type ZDHHC3 were treated with 50 ng/ml of FGF2 for 2 h, followed by analysis of ZDHHC3 phosphorylation by immunoblotting with 4G10 antibodies. As shown in Fig. 1D and E, FGF2 induced a significant increase in ZDHHC3 tyrosine phosphorylation to 118.7% ± 3.4% ($P = 0.0003$; $n = 6$) in comparison to the untreated control.

To further confirm the role of endogenous FGFR signaling in ZDHHC3 tyrosine phosphorylation, we tested whether the specific FGFR inhibitor PD173074 and the Src (which is a downstream effector of FGFR) inhibitor PP2 reduce the level of ZDHHC3 tyrosine phosphorylation. N2a cells were transfected with ZDHHC3wt cDNA and treated with 5 μM PD173074 or 10 μM PP2 for 2 h. The inactive PP2 analogue PP3 was used as

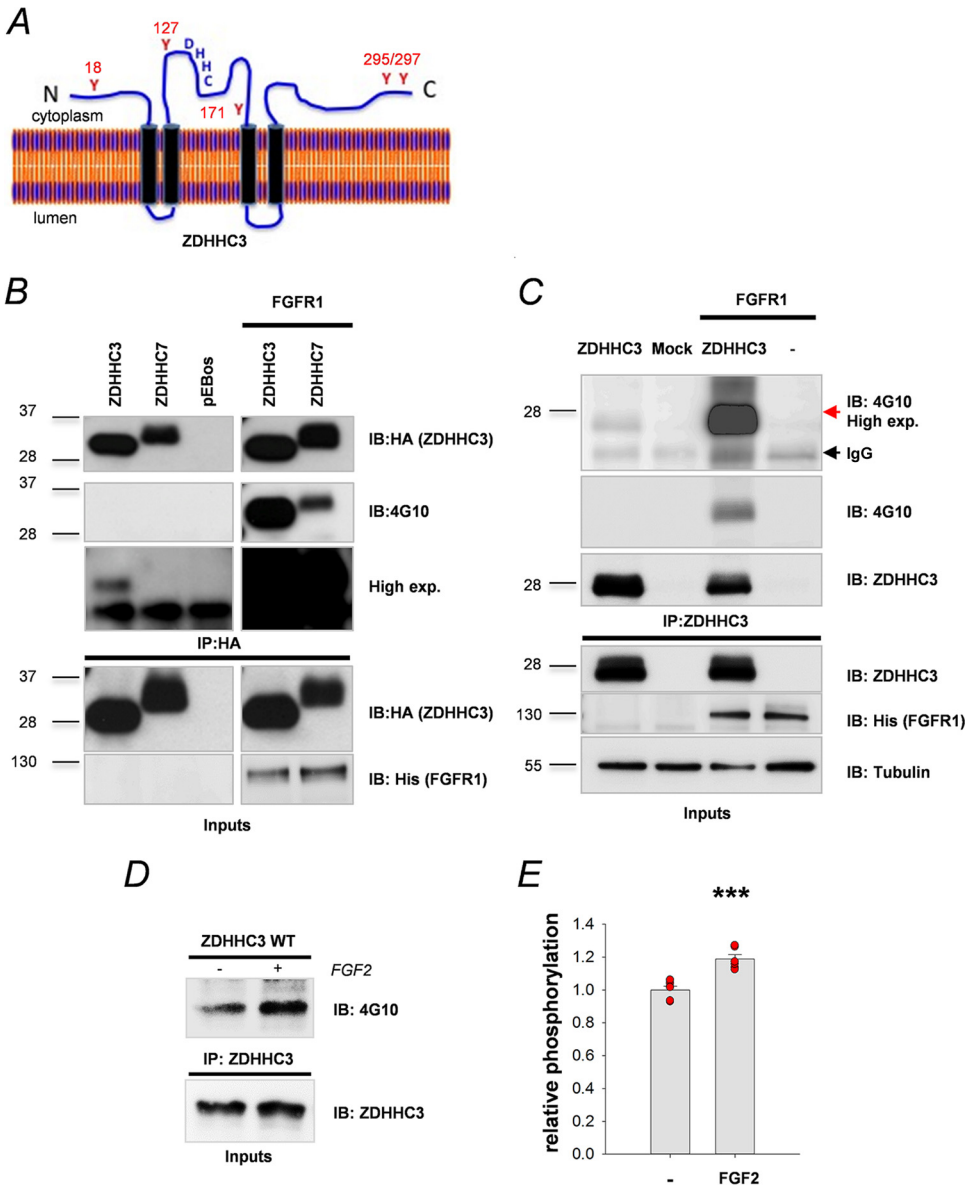

FIG 1 FGFR1 induces ZDHHC3 tyrosine phosphorylation in N2a cells. (A) Topology of ZDHHC3. DHHC indicates the conserved catalytic cysteine-rich domain. Putative tyrosine phosphorylation sites (Y) facing the cytoplasm and their positions are shown in red. (B) HA-tagged ZDHHC3 and ZDHHC7 were transfected in N2a cells alone or together with His-tagged FGFR1, immunoprecipitated with anti-HA antibodies, and analyzed by IB with antiphosphotyrosine (4G10) or anti-HA antibody. Expression (exp.) of FGFR1 was confirmed by IB. Molecular masses (in kilodaltons) are shown on the left. (C) After transfection of N2a cells, untagged ZDHHC3 was immunoprecipitated with anti-ZDHHC3 antibody and analyzed by IB with antiphosphotyrosine (4G10) or anti-ZDHHC3 antibody. Expression of FGFR1 was confirmed by IB. Expression of tubulin was used as an internal control. Molecular masses (in kilodaltons) are shown on the left. Black arrow, phosphorylated ZDHHC3; red arrow, light chains of immunoglobulin G (IgG; used for IP). (D) N2a cells expressing untagged ZDHHC3 were treated with 50 ng/ml of FGF2 or vehicle for 1 h, followed by IB analysis with antiphosphotyrosine (4G10) or anti-ZDHHC3 antibody. (E) Statistical evaluation of FGF2-mediated ZDHHC3 phosphorylation. The bars represent means plus SEM. Dots represent values obtained in individual experiments. ***, $P = 0.0003$ ($n = 6$).

a negative control. The ZDHHC3 tyrosine phosphorylation level for untreated cells was set to 1. As shown in Fig. 2A and C, PD173074 significantly ($P = 0.046$) reduced the level of ZDHHC3 tyrosine phosphorylation to 0.64 ± 0.06. Interestingly, PP2 application resulted in an even more considerable reduction of tyrosine phosphorylation (0.46 ± 0.05; $P = 0.001$) (Fig. 2B and C). Coapplication of PD173074 and PP2 displayed a cumulative effect on ZDHHC3 tyrosine phosphorylation (Fig. 2A and C).

Interestingly, overexpression of Src kinase raised the level of ZDHHC3wt tyrosine phosphorylation by 22.05- ± 3.54-fold, confirming the data obtained with PP2 treatment. However, the intensities of the detected bands always displayed greater phosphorylation of ZDHHC3 by FGFR1 than by Src kinase, as is evident in Fig. 2D, lanes 3 and 4, and E. Taken together, these data show that ZDHHC3wt contains regulatory tyrosine residues that can be phosphorylated upon activation of FGFR and/or Src signaling.

ZDHHC3 is phosphorylated by FGFR1 and Src at tyrosine residues 18, 295, and 297. To identify which of five putative ty-

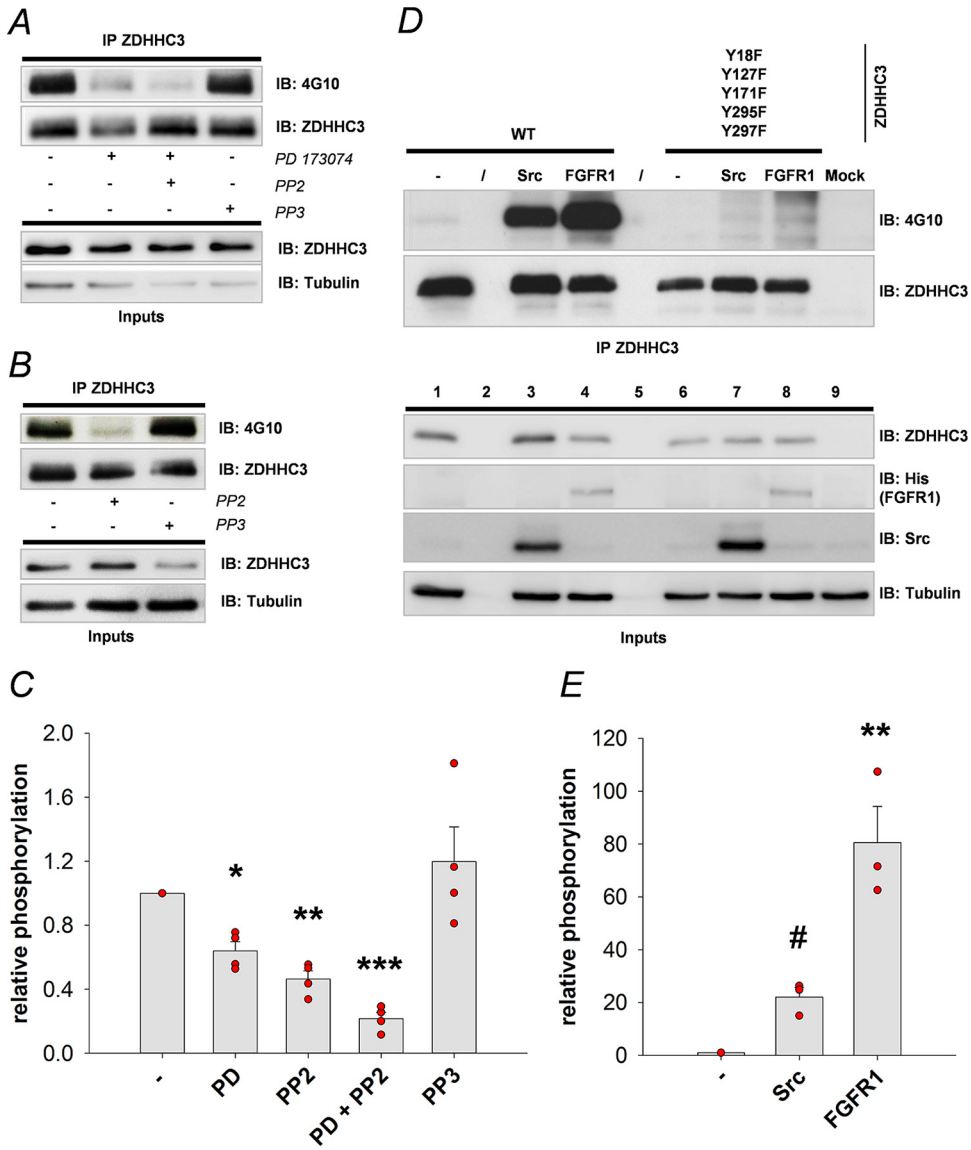

FIG 2 ZDHHC3 tyrosine phosphorylation is regulated by both FGFR and Src kinases. (A) N2a cells were transfected with ZDHHC3 and treated for 2 h with the FGFR inhibitor PD173074 (5 μM) alone or together with the Src inhibitor PP2 (10 μM). An inactive analogue of PP2 (PP3) (10 μM) was used as a negative control. Tyrosine phosphorylation of immunoprecipitated ZDHHC3 was assessed by IB with 4G10 antibody. (B) ZDHHC3 tyrosine phosphorylation after 2-h application of PP2 (10 μM) or PP3 (10 μM). (C) Statistical evaluation of ZDHHC3 tyrosine phosphorylation calculated as the 4G10/DHHC3 ratio shown in panels A and B. The bars represent means plus SEM. *, $P = 0.046$; **, $P = 0.001$; ***, $P < 0.001$ in comparison to the ZDHHC3wt untreated control group, normalized to 1; $n = 4$. (D) Tyrosine phosphorylation of ZDHHC3wt or the Y18F-Y127F-Y171F-Y295F-Y297F mutant expressed alone or together with Src or FGFR1. (E) Statistical evaluation of ZDHHC3wt tyrosine phosphorylation as shown in panel D. **, $P = 0.006$. Also shown is a comparison to the ZDHHC3wt-plus-FGFR1 group (#, $P = 0.013$; $n = 3$). (C and E) One-way RM ANOVA with the Holm-Sidak *post hoc* test was used to compare the groups. Dots represent values obtained in individual experiments.

rosines present in the ZDHHC3 cytoplasmic domain are substrates of FGFR1 and which are substrates of Src kinase, we performed site-directed mutagenesis, replacing tyrosines with phenylalanines. We first replaced all potential tyrosine phosphorylation sites, creating the ZDHHC3/Y18F-Y127F-Y171F-Y295F-Y297F mutant, and tested its ability to respond to FGFR1 or Src kinase in comparison with ZDHHC3wt. For that, ZDHHC3wt and ZDHHC3/Y18F-Y127F-Y171F-Y295F-Y297F were transfected into N2a cells alone or cotransfected with FGFR1 or Src. As shown in Fig. 2D, ZDHHC3/Y18F-Y127F-Y171F-Y295F-Y297F could not be tyrosine phosphorylated by FGFR1 or by Src, indicating that their target sites had been removed (Fig. 2D, lanes 6 to 8).

In order to identify the specific tyrosines responding to FGFR1 versus Src, we mutated single tyrosine sites, obtaining the ZDHHC3/Y18F, ZDHHC3/Y127F, ZDHHC3/Y171F, and ZDHHC3/Y295F-Y295F mutants. First, we expressed the mutants alone and evaluated the basal levels of tyrosine phosphorylation. As shown in Fig. 3A and B, phosphorylation of the ZDHHC3/Y18F and ZDHHC3/Y295F-297F mutants was dramatically reduced to 0.078 ± 0.031 and 0.119 ± 0.023, respectively, from the ZDHHC3wt level ($n = 4$; $P < 0.05$), while mutation of Y127

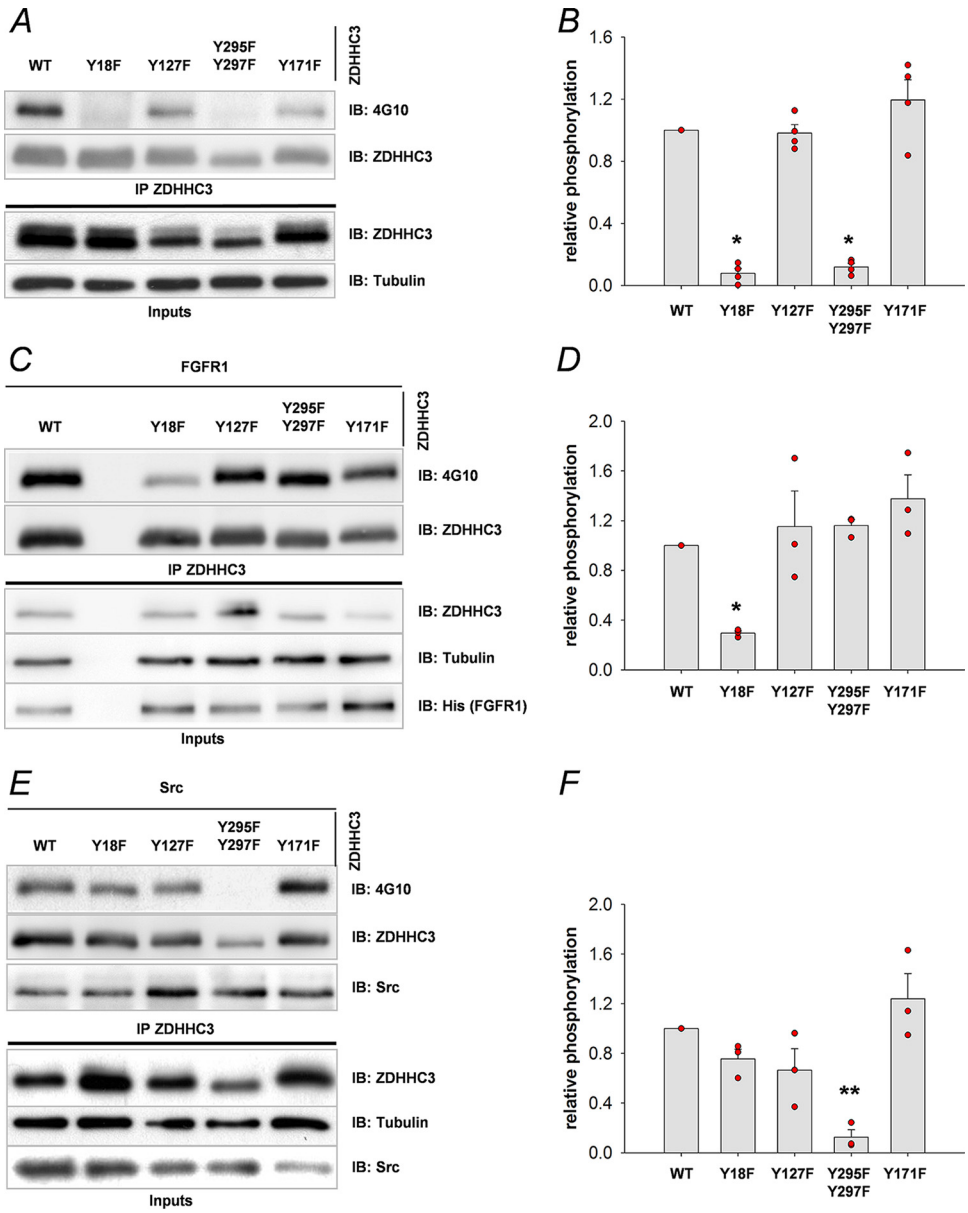

FIG 3 Tyrosine phosphorylation of ZDHHC3 single-tyrosine mutants. Shown is tyrosine phosphorylation of immunoprecipitated ZDHHC3wt or the single-tyrosine mutants ZDHHC3/Y18F, ZDHHC3/Y127F, ZDHHC3/Y295F-Y297F, and ZDHHC3/Y171F expressed alone (A and B) or coexpressed with FGFR1 (C and D) or Src (E and F) in N2a cells. Representative IBs (A, C, and E) and related graphs with statistical evaluation (B, D, and F) are shown. ZDHHC3 tyrosine phosphorylation was calculated as for Fig. 1. The bars represent means plus SEM. *, $P < 0.05$ (B); *, $P < 0.05$ (D); **, $P = 0.001$ (F) in comparison to ZDHHC3wt. For statistical comparisons, RM ANOVA on ranks followed by the Student-Newman-Keuls method ($n = 4$) (B) or one-way RM ANOVA with the Holm-Sidak *post hoc* test ($n = 3$) (D and F) was used. Dots (B, D, and F) represent values obtained in individual experiments.

and Y171 had no effect on ZDHHC3 phosphorylation (0.982 ± 0.053 and 1.195 ± 0.129, respectively). Next, we analyzed tyrosine phosphorylation of ZDHHC3 single mutants cotransfected with either FGFR1 (Fig. 3C and D) or Src (Fig. 3E and F). We found that mutation of Y18 caused a significant ($P = 0.041$) decrease of FGFR1-induced ZDHHC3 phosphorylation (to 0.295 ± 0.017 from the ZDHHC3wt level; $n = 3$), while Src-mediated phosphorylation was highly reduced in the ZDHHC3/Y295F-Y297F mutant (0.126 ± 0.059) compared with ZDHHC3wt ($P = 0.001$).

To investigate the roles of individual tyrosine sites in more detail, we generated the following mutants: ZDHHC3/Y127F-Y171F-Y295F-Y297F, ZDHHC3/Y18F-Y171F-Y295F-Y297F, ZDHHC3/Y18F-Y127F-Y295F-Y297F, and ZDHHC3/Y18F-Y127F-Y171F carrying nonmutated Y18, Y127, Y171, or Y295 and Y297 residues, respectively. Phosphorylation analysis of the newly generated ZDHHC3 mutants in N2a cells showed that a single remaining tyrosine site was not sufficient to rescue the basal level of tyrosine phosphorylation, as shown in Fig. 4A. To test whether FGFR1-mediated signaling and Src can target a different phosphorylation site(s) within ZDHHC3, N2a cells expressing triple mutants were cotransfected with FGFR1 (Fig. 4B

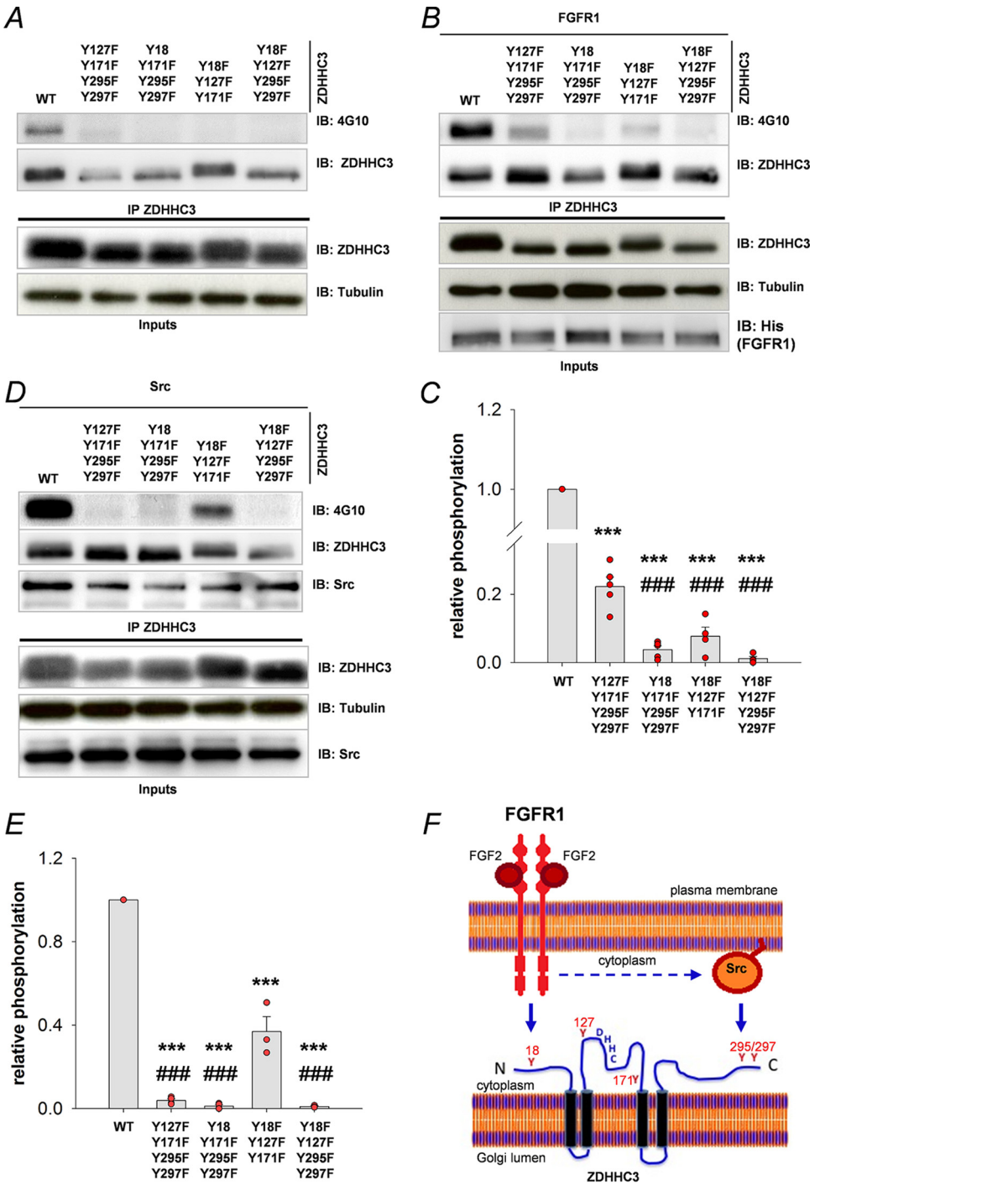

FIG 4 Tyrosine phosphorylation of ZDHHC3 triple-tyrosine mutants. (A to E) Tyrosine phosphorylation of immunoprecipitated ZDHHC3wt or the triple-tyrosine mutants ZDHHC3/Y127F-Y171F-Y295F-Y297F, ZDHHC3/Y18F-Y171F-Y295F-Y297F, ZDHHC3/Y18F-Y127F-Y171F, and ZDHHC3/Y18F-Y127F-Y295F-Y297F expressed alone (A) or coexpressed with FGFR1 (B and C) or Src (D and E) in N2a cells. The bars represent means plus SEM. ***, $P < 0.001$ in comparison to the ZDHHC3wt group; ###, $P < 0.001$ in comparison to the ZDHHC3/Y127F-Y171F-Y295F-Y297F (C) or ZDHHC3/Y18F-Y127F-Y171F (E) group (one-way RM ANOVA with Holm-Sidak *post hoc* test; $n = 4$ or 5 [C]; $n = 3$ or 4 [E]). (F) Model of site-specific ZDHHC3 tyrosine phosphorylation by FGFR1 and/or Src. Y18 (on the N terminus) is phosphorylated in response to FGFR1 activation, while Y295 and Y297 (on the C terminus) are phosphorylated directly by the Src pathway. Since FGFR may activate Src kinase, it may also phosphorylate Y295 and Y297 through Src. Dots (C and E) represent values obtained in individual experiments.

and C) or Src (Fig. 4D and E). Upon FGFR1 overexpression, ZDHHC3/Y127F-Y171F-Y295F-Y297F and ZDHHC3/Y18F-Y127F-Y171F showed mild phosphorylation compared with ZDHHC3wt, where the mutant with intact Y18 was significantly more phosphorylated than the other triple mutants ($P <$ 0.001; $n = 4$ or 5). Upon Src overexpression, only ZDHHC3/Y18F-Y127F-Y171F showed increased tyrosine phosphorylation in comparison with the other mutants ($P < 0.001$; $n = 3$ or

4), suggesting Y295 and Y297 are preferential phosphorylation sites for Src.

In summary, these data indicate that tyrosines 295 and 297 are specific substrates of Src and tyrosine 18 is the major target for FGFR1-mediated signaling, while tyrosines 127 and 171 respond to neither FGFR1 nor Src kinase (Fig. 4F shows the scheme). The moderate activation of phosphorylation observed in ZDHHC3/Y18F (Fig. 3C) and ZDHHC3/Y18F-Y127F-Y171F (Fig. 4B) upon FGFR1 overexpression suggests that other FGFR1 downstream effectors may also target tyrosines 295 and 297.

Phosphorylation-deficient ZDHHC3 palmitoylates NCAM180 with higher efficiency than the wt form. Taking into account that FGFR signaling is involved in NCAM palmitoylation (18), we asked whether tyrosine phosphorylation could play a role in regulating ZDHHC3 enzymatic activity toward NCAM. For that purpose, we carried out [^{3}H]palmitate labeling of NCAM180 in the presence of ZDHHC3wt or its ZDHHC3 tyrosine-defective mutants: ZDHHC3/Y127F-Y171F-Y295F-Y297F (i.e., Y18 intact), ZDHHC3/Y18F-Y127F-Y171F (i.e., Y295 and Y297 intact), and ZDHHC3/Y18F-Y127F-Y171F-Y295F-Y297F. As a negative control, we used a catalytically inactive dominant-negative C157S mutant of ZDHHC3. In accordance with our previous findings, NCAM palmitoylation was increased by overexpression of ZDHHC3wt (18) but not by a catalytically inactive ZDHHC3 mutant (25) (Fig. 5A and B). The tyrosine-defective ZDHHC3/Y127F-Y171F-Y295F-Y297F mutant (with intact Y18 representing a preferential phosphorylation site for FGFR1) (Fig. 4B) further increased NCAM palmitoylation, while ZDHHC3/Y18F-Y127F-Y171F (containing Y295 and Y297 and preferentially phosphorylated upon Src overexpression) (Fig. 4D) possessed the same enzymatic activity as ZDHHC3wt (Fig. 5B). Interestingly, the full tyrosine mutant ZDHHC3/Y18F-Y127F-Y171F-Y295F-Y297F also showed an increased level of palmitoylation compared to ZDHHC3wt, although to a lesser extent than the mutant with intact Y18. These data demonstrate that Y295 and Y297 negatively regulate ZDHHC3 catalytic activity toward its substrate, NCAM, whereas Y18 may facilitate palmitoylation. This suggests that tyrosine phosphorylation of ZDHHC3 by Src can retard NCAM palmitoylation, while FGFR1 may promote it.

Enhanced substrate palmitoylation could result from enzyme translocation within the cell, as was demonstrated for PSD-95 PAT-ZDHHC2 (50–52). To ascertain that tyrosine replacement would not result in cellular mislocalization of the ZDHHC3 enzyme, we generated a GFP-tagged version of ZDHHC3/Y18F-Y127F-Y171F-Y295F-Y297F and analyzed the localization of the mutant in N2a cells by confocal microscopy. GFP-ZDHHC3/Y18F-Y127F-Y171F-Y295F-Y297F remained in the Golgi compartment and was colocalized with the Golgi marker GM130 (see Fig. S2 in the supplemental material).

FGF2 treatment enhances NCAM palmitoylation *in vivo*. Having demonstrated that stimulation of FGFR with FGF2 promotes tyrosine phosphorylation of ZDHHC3 (Fig. 1D and E) and facilitates NCAM palmitoylation *in vitro* (18), we next determined whether NCAM palmitoylation is regulated by FGF2-FGFR signaling *in vivo* and also analyzed the possible role of ZDHHC3 phosphorylation in this process. For that, FGF2 was injected s.c. into the brains of C57BL6J mice, followed by palmitoylation analysis of endogenous NCAMs using ABE chemistry. This technique does not require metabolic labeling of cells or tissues and therefore permits identification of palmitoylation of proteins in their native surroundings. The ABE technique is based on the cleavage of thioester linkages between cysteines and palmitates by hydroxylamine (NH_2OH). Cleavage of the thioester link allows the specific incorporation of a biotinylated analogue of palmitate (HPDP-biotin) into the newly available thiol group and permits detection of biotinylated palmitate analogues by Western blotting. Using this approach, we could demonstrate *in vivo* palmitoylation of endogenous NCAM140 and -180 in mouse brain (Fig. 5C). FGF2 treatment significantly increased the palmitoylation levels of both endogenous NCAM140 and NCAM180 by 12.8% ± 1.3% ($n = 4$) and 37.3% ± 1.3%, respectively (Fig. 5D). The effect of FGF2 was specific to NCAM, since the level of PSD95 palmitoylation was not changed (Fig. 5C). Also, the general level of the palmitoylated brain proteins assayed by silver staining was not altered after FGF2 treatment (see Fig. S3 in the supplemental material).

To assess whether FGF2 induces ZDHHC3 tyrosine phosphorylation *in vivo*, brain lysates from FGF2-injected mice were subjected to IP using anti-ZDHHC3 antibodies, followed by IB with antiphosphotyrosine antibody (4G10). This experiment confirmed tyrosine phosphorylation of ZDHHC3 *in vivo* (Fig. 5E). Interestingly, while FGF2 treatment failed to increase tyrosine phosphorylation of ZDHHC3 monomers, it promoted tyrosine phosphorylation of ZDHHC3 dimers, very reproducibly revealed as complexes of about 60 kDa (Fig. 5E). It has been previously demonstrated that ZDHHC3 can form homodimers and that dimerization can be involved in the regulation of DHHC functions (53). Our results suggest possible interplay between activity-dependent DHHC3 phosphorylation and dimerization. This is an interesting observation that will be followed up in future studies. In summary, *in vivo* administration of FGF2 stimulated an increase in NCAM palmitoylation that was accompanied by increased phosphorylation of endogenous ZDHHC3, suggesting that dynamic ZDHHC phosphorylation could represent a novel mechanism regulating DHHC activity, not only in a recombinant system (Fig. 1) but also *in vivo*.

Y295 and Y297 replacement raises ZDHHC3 autopalmitoylation and enhances its interaction with NCAM. A common feature of ZDHHC PATs is autopalmitoylation, a step preceding palmitate transfer to target proteins (35). We asked whether the higher efficiency in palmitoylating NCAM acquired by the tyrosine-deficient mutant correlates with a higher degree of self-palmitoylation. To evaluate palmitic acid uptake by the different ZDHHC3 molecules, we used the nonradioactive Click-iT method, with some modifications (see Materials and Methods and Fig. S4 in the supplemental material). By this approach, palmitoylated ZDHHC3wt enriched by streptavidin-Sepharose pulldown was readily detected by anti-ZDHHC3 antibodies (Fig. 6A, lanes 3, 4, and 8). No bands were visible in the samples purified with streptavidin if palmitic acid-azide or biotin-alkyne were replaced by vehicle (Fig. 6A, lanes 1 and 2). Introduction of the dominant-negative mutation C157S abolished the autoacylation property in both ZDHHC3wt and the ZDHHC3/Y18F-Y127F-Y171F-Y295F-Y297F mutant (Fig. 6A, lanes 10 and 11). Since calnexin is palmitoylated by ZDHHC6 but not ZDHHC3 (54), we assayed calnexin palmitoylation by staining the same blots with anticalnexin antibodies and used this signal as an internal control. Next, we analyzed the degree of ZDHHC3 autopalmitoylation, quantified relative to the total amount of proteins recovered after the Click-iT procedure, and found that the absence of all five tyrosines (in ZDHHC3/Y18F-Y127F-Y171F-Y295F-Y297F) increased auto-

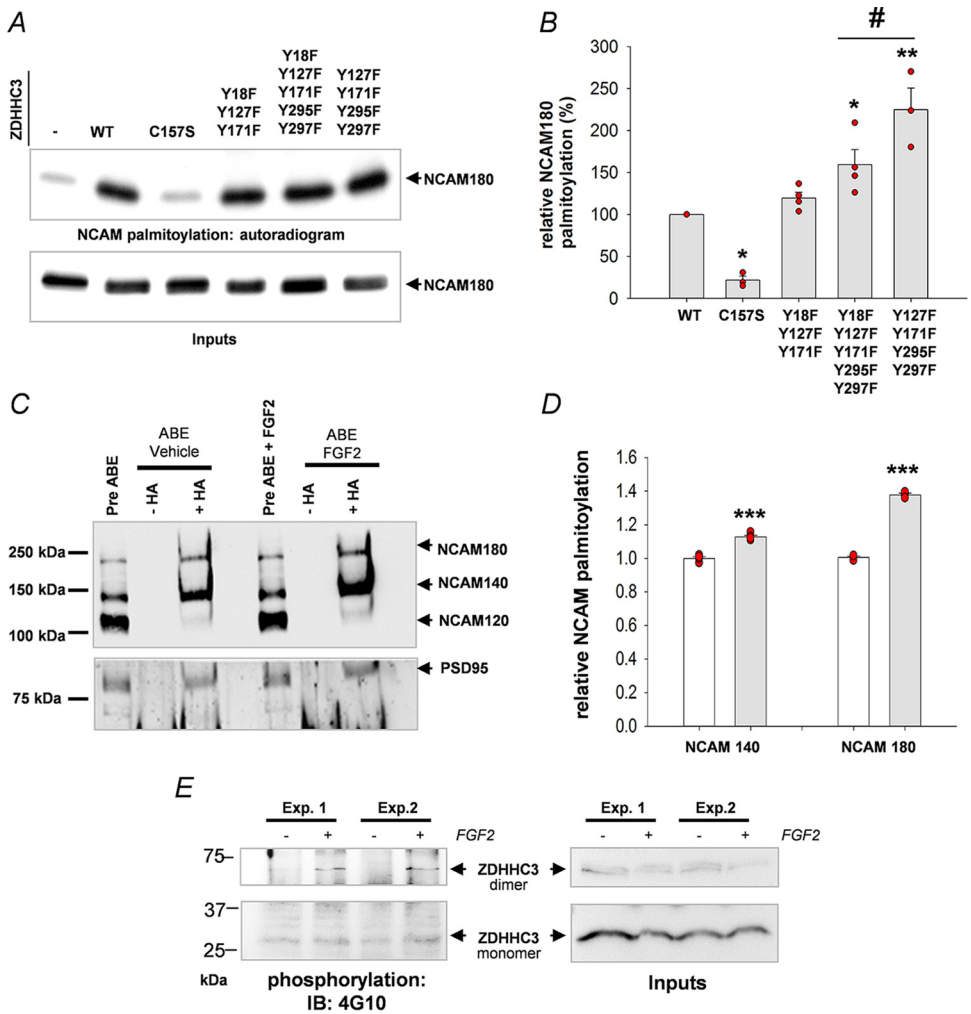

FIG 5 Palmitoylation of NCAM180 by ZDHHC3wt versus phosphorylation-deficient mutants and role of FGFR activation in NCAM palmitoylation and ZDHHC3 phosphorylation *in vivo*. (A) N2a cells were cotransfected with NCAM180 and ZDHHC3wt, its dominant-negative mutant C157S, or phosphorylation-deficient mutants; labeled with [^{3}H]palmitate; and subjected to immunoprecipitation with anti-NCAM antibody, followed by SDS-PAGE and fluorography. (B) The intensity of the NCAM180 [^{3}H]palmitate labeling was assessed by densitometry of fluorograms relative to protein levels estimated by immunoblotting. The value for cells transfected with ZDHHC3wt was set to 100%. The bars represent means plus SEM ($n = 3$ or 4). The statistically significant difference between ZDHHC3wt and ZDHHC3/C157S ($P = 0.022$), ZDHHC3/Y127F-Y171F-Y295F-Y297F ($P = 0.001$), or ZDHHC3/Y18F-Y127F-Y171F-Y295F-Y297F ($P = 0.046$) is indicated (*, $P < 0.05$; **, $P < 0.01$), as well as that between ZDHHC3/Y127F-Y171F-Y295F-Y297F and ZDHHC3/Y18F-Y127F-Y171F-Y295F-Y297F (#, $P = 0.035$) (one-way RM ANOVA with Holm-Sidak *post hoc* test). (C) Representative ABE analysis of NCAM palmitoylation in mouse brain treated with vehicle/FGF2, followed by SDS-PAGE and Western blotting. The samples without hydroxylamine (− HA) functioned as a negative control for specific palmitoyl biotinylation. Shown is a representative blot from at least three independent experiments. (D) Statistical evaluation of NCAM140 and NCAM180 palmitoylation. Injection of FGF2 increases palmitoylation of endogenous NCAM140 and NCAM180 by 12.8% ± 1.3% ($n = 4$) and by 37.3% ± 1.3% ($n = 3$), respectively. The bars represent means plus SEM. ***, $P < 0.001$. (E) Representative blots showing tyrosine phosphorylation (left) and expression (right) of endogenous ZDHHC3 in mouse brain after s.c. injection of FGF2 or vehicle in two independent experiments (Exp.). Administration of FGF2 facilitates phosphorylation of dimeric, ~60-kDa ZDHHC3 (top) rather than its monomeric form (bottom). Dots (B and D) represent values obtained in individual experiments.

palmitoylation of the enzyme 1.926- ± 0.106-fold ($P < 0.001$; $n = 11$) (Fig. 6A, lanes 7 and 9, and C). We next analyzed the ZDHHC3/Y127F-Y171F-Y295F-Y297F and ZDHHC3/Y18F-Y127F-Y171F mutants, aiming to dissect the respective roles of Y18 or Y295 and Y297 for ZDHHC3 autopalmitoylation. We observed that palmitate uptake by ZDHHC3/Y127-Y171F-Y295F-Y297F, with the only Y18 intact, was significantly higher ($n = 4$; $P < 0.001$) than palmitate uptake by ZDHHC3wt, reaching the levels of the full ZDHHC3 tyrosine mutant autopalmitoylation (Fig. 6A, lane 5, and C). Conversely, palmitate uptake by the ZDHHC3/Y18F-Y127F-Y171F mutant ($n = 4$) was comparable to the levels of ZDHHC3wt autopalmitoylation (Fig. 6A, lane 6, and C). These data suggest that tyrosines 295 and 297 have an inhibitory effect on ZDHHC3 autopalmitoylation, since their mutation clearly favored ZDHHC3 autopalmitoylation. Restoring only tyrosine 18 had no influence on ZDHHC3 autopalmitoylation, indicating that phosphorylation of this residue is not directly involved in regulation of ZDHHC3 autopalmitoylation.

Although enzyme-substrate complexes are usually characterized by a short half-life, we aimed to explore whether the higher degree of autopalmitoylation of the full tyrosine mutant would result in a higher binding affinity of ZDHHC3 to its substrate,

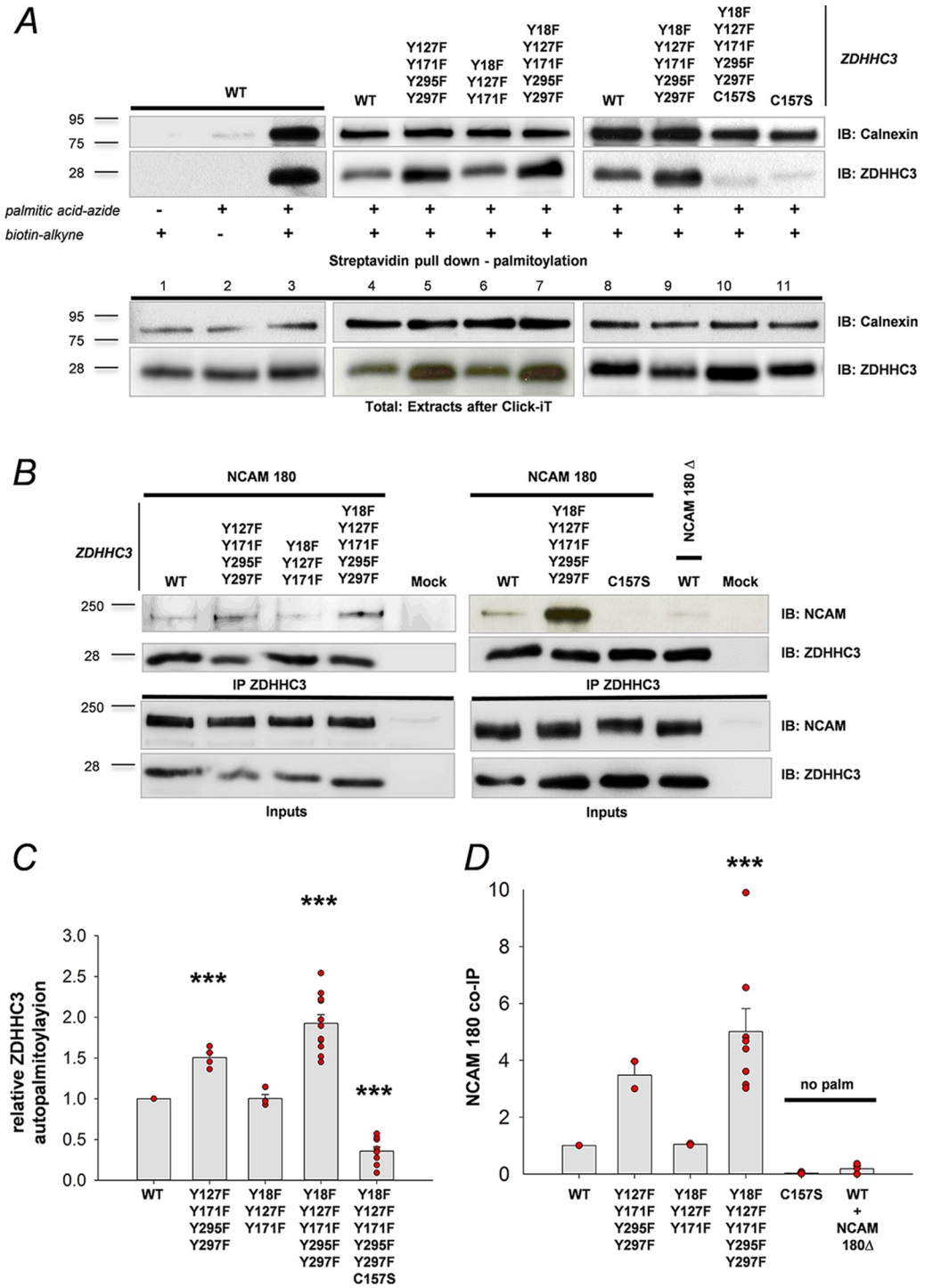

FIG 6 Mutation of tyrosines enhances ZDHHC3 autopalmitoylation and its interaction with NCAM. (A) Autopalmitoylation of transfected wt or mutant ZDHHC3 into N2a cells was analyzed by Click-iT chemistry. Calnexin served as an internal positive control. As a negative control, a click reaction was performed without palmitic acid-azide or biotin-alkyne. Palmitoylated ZDHHC3 or calnexin pulled down by streptavidin-Sepharose beads was detected by IB with specific antibodies. The relative total amount of these proteins after the Click-iT reaction was determined by IB of extracts, shown below the line. (B) NCAM180 or NCAM180Δ coimmunoprecipitating with wt or mutant ZDHHC3 was analyzed after ZDHHC3 IP by IB with anti-NCAM antibodies. The amount of ZDHHC3 in IP was detected on the same membrane. ZDHHC3 and NCAM180 expression was confirmed by IB of the lysates. (C and D) Statistical evaluation of ZDHHC3 autopalmitoylation, calculated as the palmitoylated/total ratio. The bars represent means plus SEM. ***, $P < 0.001$ in comparison to ZDHHC3wt (one-way RM ANOVA with Holm-Sidak posttest). Dots (C and D) represent values obtained in individual experiments.

NCAM. To answer this question, we applied co-IP analysis. First, we found that NCAM180 coexpressed in N2a cells with ZDHHC3 is pulled down together with it, suggesting an interaction between the enzyme and its substrate. The observed binding was not an *in vitro* artifact, as shown by lack of NCAM coimmunoprecipitated with ZDHHC3 from the mixture of two lysates derived from cells independently transfected with either ZDHHC3 or NCAM (see Fig. S5 in the supplemental material). Then, we compared the amount of NCAM180 coimmunoprecipitated with either ZDHHC3wt or the ZDHHC3/Y18F-Y127F-Y171F-Y295F-Y297F mutant, calculated in relation to the amount of ZDHHC3 in IP and the NCAM expression level. We found that ZDHHC3/Y18F-Y127F-Y171F-Y295F-Y297F pulls down 5.016 ± 0.804 times more NCAM180 than ZDHHC3wt does ($n = 8$; $P < 0.001$) (Fig. 6B and D). The catalytic-defective ZDHHC3/C157S mutant, used as a negative control, failed to coimmunoprecipitate NCAM180, confirming the requirement of autopalmitoylation for interaction. Analogously, interaction between ZDHHC3 and palmitoylation-deficient NCAM180 (NCAM180Δ) was almost completely abolished (Fig. 6B, right). Similarly to the full tyrosine mutant, the ZDHHC3/Y127-Y171F-Y295F-Y297F mutant with intact Y18, but not the ZDHHC3/Y18F-Y127F-Y171F mutant with intact Y295 and Y297, had a tendency toward a higher degree of interaction with NCAM180 than ZDHHC3wt. In summary, these data show that tyrosines 295 and 297 represent a negative regulator of autopalmitoylation, as well as interaction of ZDHHC3 with its substrate, NCAM180, which is in agreement with their involvement in the regulation of ZDHHC3 enzymatic activity toward NCAM (Fig. 5).

Role of Src kinase in ZDHHC3 phosphorylation. In our experiments, we observed that Src controls tyrosine phosphorylation of ZDHHC3. In view of the evidence that Src kinase can interact with its substrates (55–57), we hypothesized that it can interact with ZDHHC3. Since N2a cells express Src endogenously, we verified our hypothesis using a mouse embryonic fibroblast (MEF) line (also called $SYF^{-/-}$) that is deficient in the three most prominent members of the Src family kinases (Src, Fyn, and Yes). $SYF^{-/-}$ cells were transfected with ZDHHC3 alone or together with Src for 24 h and lysed, and the protein extracts obtained were subjected to IP with anti-ZDHHC3 antibodies. The collected immunocomplexes were then analyzed by IB with antibodies directed against Src. We observed that Src cotransfected with ZDHHC3 was coimmunoprecipitated together with ZDHHC3, suggesting an interaction between the proteins (Fig. 7A). Interaction specificity was confirmed by coimmunoprecipitation experiments performed with mixed lysates from cells separately transfected with ZDHHC3 and Src (see Fig. S6 in the supplemental material).

Since Src kinase phosphorylates ZDHHC3 at tyrosines 295 and 297, which turned out to regulate the enzymatic activity of the PAT negatively, we asked next whether interaction with Src is disrupted by tyrosine mutations in ZDHHC3 or by mutation in the ZDHHC3 catalytic site. The Y18F-Y127F-Y171F-Y295F-Y297F and C157S ZDHHC3 forms were able to pull down Src, suggesting that neither tyrosine phosphorylation nor palmitate uptake at cysteine 157 is a prerequisite for the Src-ZDHHC3 interaction (Fig. 7A and B). To directly verify the role of Src in ZDHHC3 phosphorylation, we performed a radioactive *in vitro* kinase assay using purified Src proteins. As shown in Fig. 7C, Src kinase successfully transferred radioactively labeled phosphate to ZDHHC3wt, ZDHHC3/Y18F-Y127F-Y171F, and ZDHHC3/C157S, while it failed to phosphorylate ZDHHC3/Y127F-Y171F-Y295F-Y297F and ZDHHC3/Y18F-Y127F-Y171F-Y295F-Y297F mutants. These results confirm that Y295 and Y297 represent the specific direct targets of Src.

The Src SH3 domain is known to be involved in interactions with substrate proteins, and such interaction might involve the PXXP consensus sequence within the substrate (58). Analyses of the ZDHHC3 sequence revealed the presence of two prolines in positions 27 and 30 within the PPFP sequence close to its N terminus. To verify the role of the PPFP sequence as a putative Src binding domain, we changed prolines 27 and 30 into alanines, generating the following mutants: ZDHHC3/P27A-P30A, ZDHHC3/P27A-P30A-Y295F-Y297F, and ZDHHC3/P27A-P30A-Y18F-Y127F-Y171F-Y295F-Y297F. To assay whether the new mutants would lose the ability to interact with Src, we performed co-IP experiments following the same procedure described above for C157S and ZDHHC3s with tyrosine mutated. As shown in Fig. 7D, mutation of the PPFP sequence to APFA did not abolish Src-ZDHHC3 interaction, suggesting that other sites can be involved in enzyme-substrate interaction in the case of Src-mediated ZDHHC3 phosphorylation (23).

Tyrosine phosphorylation of ZDHHC3 is involved in regulation of neurite outgrowth. Palmitoylation of NCAM provides association of NCAM with lipid rafts and thus stimulates the neurite outgrowth of cultured hippocampal neurons. Since replacement of tyrosines 295 and 297 of ZDHHC3 increases autopalmitoylation of ZDHHC3 and stimulates its palmitoylating activity toward NCAM (Fig. 5), we asked whether mutant ZDHHC3 could influence neuronal morphogenesis. To answer this question, we analyzed the total length of neurites, the number of primary neurites, and the length of the longest (major) neurite in DIV2 hippocampal neurons transfected with ZDHHC3wt or the full tyrosine mutant (ZDHHC3/Y18F-Y127F-Y171F-Y295F-Y297F). Neurons at day 2 *in vitro* were identified by staining with the neuronal marker β-tubulin III (Fig. 8A). Transfected neurons were identified by cotransfection with a vector encoding EGFP. As a baseline control, we used neurons cotransfected with EGFP and an empty pcDNA3.0 vector. The mean values in wt and tyrosine mutant ZDHHC3-transfected groups within each transfection were normalized using the mean values in the control group (set to 100%). We found that overexpression of the tyrosine mutant ZDHHC3/Y18F-Y127F-Y171F-Y295F-Y297F caused a statistically significant ($n = 4$; $P = 0.027$) 28.4% ± 7.1% increase in the total length of neurites compared to the baseline control group (with a mean total neurite length of 162 ± 14 μm), as well as relative to the ZDHHC3wt group ($P = 0.022$) (Fig. 8B). The increase in the total neurite length was mainly due to the increase in the number of neurites, which was significantly ($P = 0.006$ and $P = 0.011$) higher in ZDHHC3/Y18F-Y127F-Y171F-Y295F-Y297F-transfected neurons (118.73% ± 4.81%) than in ZDHHC3wt-transfected cells (95.73% ± 2.79%) or control neurons (100%) (Fig. 8C). There was also a slight tendency toward an increase in the length of the longest neurite in the ZDHHC3/Y18F-Y127F-Y171F-Y295F-Y297F group, but it was not significant (Fig. 8D).

DISCUSSION

In this study, we uncovered a mechanism of ZDHHC3 regulation through its tyrosine phosphorylation by either receptor or

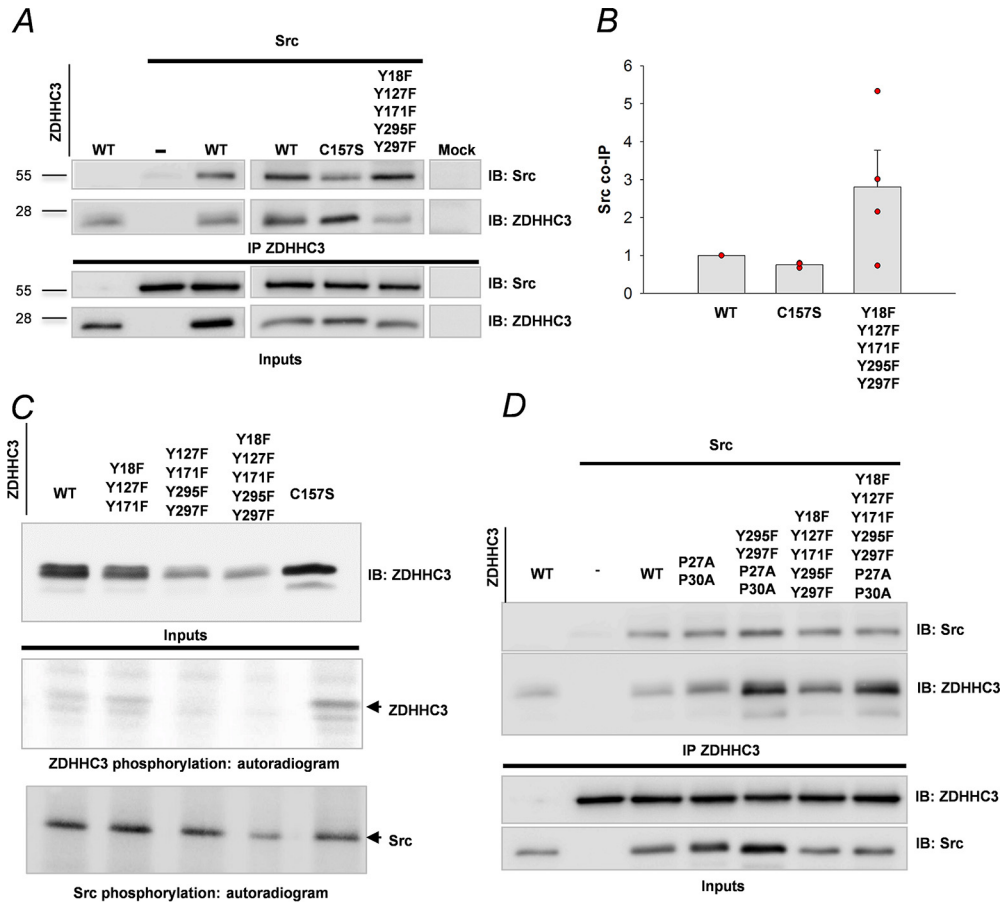

FIG 7 Src interacts with and phosphorylates ZDHHC3. (A) Src and ZDHHC3wt or the indicated mutant forms were transfected in SYF$^{-/-}$ cells separately or together. After immunoprecipitation of ZDHHC3, the amount of Src pulled down together with ZDHHC3 was analyzed by WB with anti-Src antibodies. Expression of ZDHHC3 and Src was confirmed by WB of the extracts with specific antibodies, shown below the line. (B) Statistical evaluation of Src co-IP. The bars represent means plus SEM. $n = 3$ for the second group; $n = 4$ for the first and third groups. There were no significant differences between groups. Dots represent values obtained in individual experiments. (C) *In vitro* Src kinase assay. ZDHHC3wt or the indicated mutants were transfected in N2a cells. After immunoprecipitation, samples were incubated with purified Src kinase together with [γ-^{33}P]ATP, followed by SDS-PAGE and fluorography (below the line). The blot above the line shows the expression levels of the different ZDHHC3 molecules after IP. Autophosphorylation of Src is shown in the bottom blot. The data are representative of the results of three independent experiments. (D) ZDHHC3wt or mutants bearing the additional P27A-P30A mutations were transfected in N2a cells, along with Src, followed by the pulldown assay. Representative blots demonstrating expression of ZDHHC3 and Src are shown below the line.

nonreceptor tyrosine kinases. First, we identified tyrosine 18 of ZDHHC3 as the major target of FGFR1 signaling and tyrosines 295 and 297 as specific substrates for the Src kinase. Second, we demonstrated that the replacement of tyrosines 295 and 297 with phenylalanines led to enhanced ZDHHC3 autopalmitoylation, stronger ZDHHC3-NCAM interaction, and upregulation of ZDHHC3-mediated NCAM palmitoylation. Third, we found that abrogation of ZDHHC3 tyrosine phosphorylation stimulated neurite outgrowth of hippocampal neurons.

In silico analysis of ZDHHC3 and ZDHHC7 cytoplasmic domains revealed the presence of several recognition sites for known tyrosine and serine/threonine kinases (http://www.hprd.org/PhosphoMotif_finder). Due to the critical importance of FGF2-induced receptor tyrosine kinase (FGFR) for ZDHHC3 activity (18), we focused on analysis of tyrosine phosphorylation and performed experiments with cotransfection of FGFR1 and ZDHHC3 in N2a cells. We observed strong tyrosine phosphorylation of ZDHHC3 and the closely related paralog ZDHHC7. Because tyrosines present in the HA-tagged version of ZDHHC3 could be phosphorylated by FGFR1 (see Fig. S7 in the supplemental material), we had to perform all further analysis using the untagged version of ZDHHC3.

Since ZDHHC3 could be tyrosine phosphorylated by exogenous FGFR1, we expected that endogenous kinases would also target ZDHHC3. By using FGF2, the FGFR inhibitor PD173074, and the Src family member inhibitor PP2, we have shown that ZDHHC3 can be phosphorylated by endogenously expressed FGFR and Src family proteins. Notably, the observed cumulative effects of PD173074 and PP2 suggested that FGFR and Src might mediate ZDHHC3 phosphorylation independently. Accordingly, mutating all five tyrosines into phenylalanines fully prevented ZDHHC3 tyrosine phosphorylation, even under conditions of strong forced expression of FGFR1 or Src.

Single-site mutagenesis allowed us to identify tyrosines 295 and 297 as specific targets of Src and tyrosine 18 as a major target of FGFR1 signaling. However, since Src is a part of the signaling cascade activated by FGFRs (55, 57, 59, 60), we hypothesized that the mild tyrosine phosphorylation detected for tyrosines 295 and

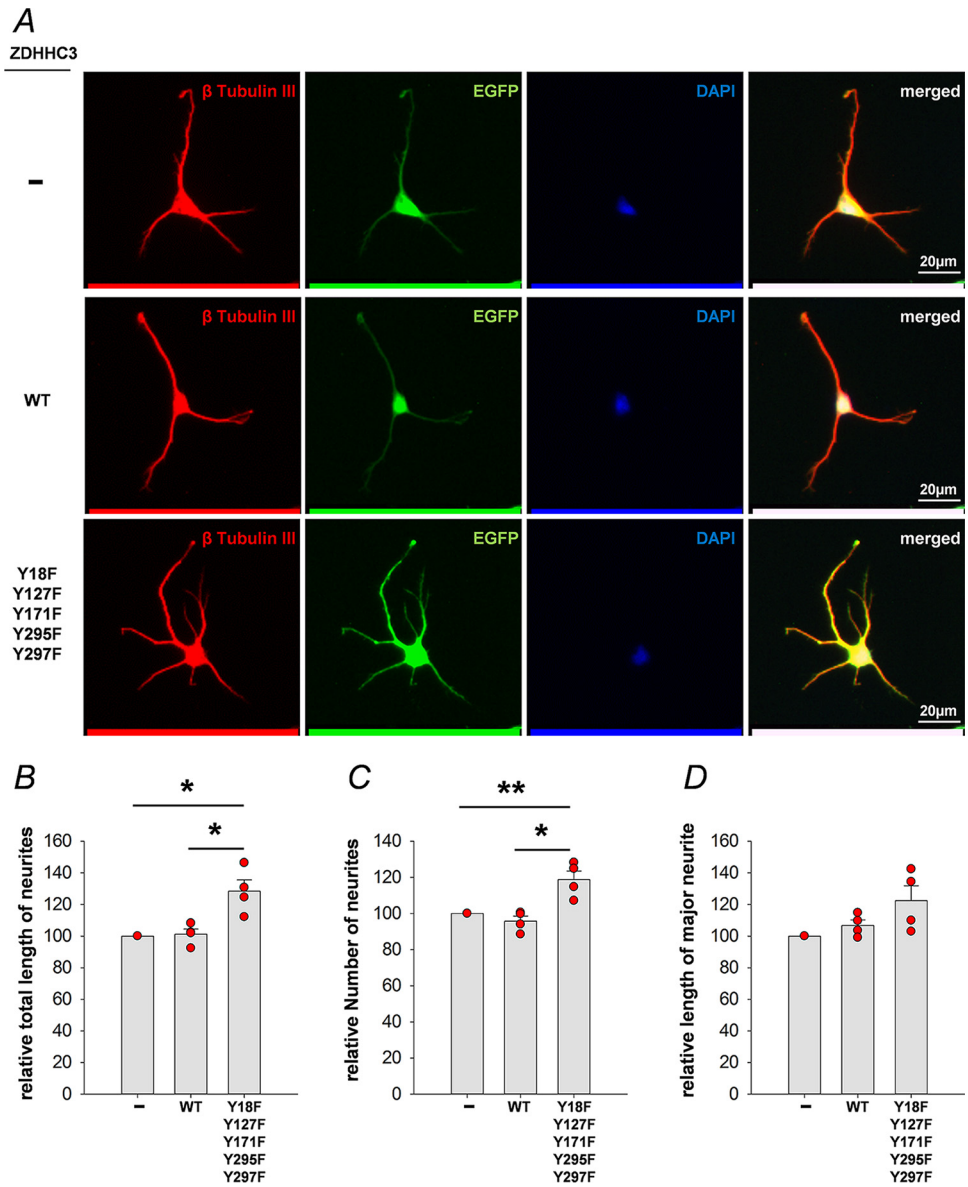

FIG 8 Mutation of tyrosines in ZDHHC3 stimulates neurite outgrowth. (A) Representative images of DIV2 hippocampal neurons cotransfected with EGFP (green channel), together with an empty vector (−; first control group), ZDHHC3wt (second group), or the ZDHHC3 tyrosine mutant (Y18F-Y127F-Y1717F-Y295F-Y297F) (third group), stained with β-tubulin III (red), and mounted with DAPI (blue)-containing medium. (B to D) Statistical evaluation of the total length of all neurites (B), the number of primary neurites (C), and the length of the longest neurite (D) of cells positive for both β-tubulin III and EGFP. The bars show means plus SEM. The mean values within each transfection were normalized to the control group (set to 100%). *, $P < 0.05$; **, $P < 0.01$ (one-way RM ANOVA with Holm-Sidak *post hoc* test). The number of culture preparations/transfections was 4; the number of coverslips was 8 (2 per transfection); and the total numbers of neurons analyzed were 358, 347, and 270 for the first, second, and third groups, respectively. Dots represent values obtained in individual experiments.

297 in the presence of exogenous FGFR1 of the ZDHHC3/Y18F mutant might be due to induced activation of endogenous Src. Interestingly, analysis of the ZDHHC3 mutants with only intact tyrosine 18 (ZDHHC3/Y127F-Y171F-Y295F-Y297F) or tyrosines 295 and 297 (ZDHHC3/Y18F-Y127F-Y171F) showed no apparent tyrosine phosphorylation by endogenous kinases, suggesting the requirement for both sites for this. Phosphorylation of ZDHHC3 could be carried out by downstream effectors of FGFR and Src or directly by these kinases. By performing an *in vitro* kinase assay, we confirmed that Src directly phosphorylates ZDHHC3 at tyrosines 295 and 297. Since Src localizes to the plasma membrane and cytoplasmic compartments, we hypothesize that phosphorylation of ZDHHC3 occurs at the Golgi compartment, where the PAT resides. Furthermore, ZDHHC3 has been detected in the post-Golgi compartment and NCAM associates with *trans*-Golgi network (TGN)-derived organelles, which may come very close to the plasma membrane (61, 62). Hence, FGFR can "meet" and tyrosine phosphorylate intracellular ZDHHC3 during trafficking by recycling endosomes to the TGN, which in turn may affect palmitoylation of NCAM. In agreement with the hypothesis of direct phosphorylation of ZDHHC3 by Src/FGFR, we found that Src interacts with ZDHHC3.

Interestingly, the interplay between this tyrosine kinase and PAT could be bidirectional. Recently, it was shown that ablation of ZDHHC3 diminishes integrin α6- and β4-dependent p-Src (Y416) activation, a process involved in cancer cell motility and invasion. This reduction was presumably the consequence of accelerated degradation of nonpalmitoylated α6 and β4, which are both ZDHHC3 substrates (30).

Incorporation of [^{3}H]palmitic acid is a reliable technique to estimate protein palmitoylation (63), and it was originally used to identify ZDHHC3 as a specific PAT for NCAM140 and -180 (18). We applied this technique to study the role of tyrosine phosphorylation in ZDHHC3 catalytic activity toward NCAM180. We found that when tyrosines Y295 and Y297 were mutated either in ZDHHC3/Y127F-Y171F-Y295F-Y297F or in the total tyrosine mutant, NCAM palmitoylation was significantly increased (Fig. 5). In combination with our finding that Y18 is preferentially phosphorylated upon FGFR1 overexpression while Y295 and Y297 represent a target for Src (Fig. 4), this suggests that phosphorylation of Y295 and Y297 by Src has an inhibitory effect on enzymatic ZDHHC3 activity toward its substrate (a "switch off" effect), while FGFR1-mediated phosphorylation of Y18 can overcome such inhibition (a "switch on" effect). This model fits well with our previous observation that FGF2-FGFR signaling upregulates NCAM palmitoylation in cultured cells (18). Moreover, the results of the present study demonstrate that FGF2-FGFR signaling facilitates ZDHHC3 tyrosine phosphorylation and triggers NCAM palmitoylation *in vivo*, demonstrating the physiological relevance of regulated ZDHHC3 phosphorylation.

It has been reported that FGFR can modulate Src activity and that such modulation largely depends on the cell type and the phase of the cell cycle, as well as on the duration of FGF exposure to the cell (64–68). Thus, interplay between FGFR-mediated Src-independent phosphorylation of ZDHHC3 (switch on) and Src-mediated phosphorylation of Y295/297 (switch off) could represent a molecular mechanism responsible for the fine-tuning of ZDHHC3 activity.

Autoacylation is a feature of multiple ZDHHC enzymes (69–71), and recent studies have shown that autopalmitoylated ZDHHC3 and ZDHHC2 represent an intermediate reaction state for palmitate transfer to the target protein (35). The identification of regulatory tyrosines on ZDHHC3 led us to investigate whether tyrosine phosphorylation could influence autopalmitoylation. Using the nonradioactive Click-iT method, we observed upregulated autopalmitoylation of ZDHHC3/Y127F-Y171F-Y295F-Y297F (with intact Y18 only) but not of ZDHHC3/Y18F-Y127F-Y171F (with Y295 and Y297 intact), suggesting that tyrosine phosphorylation, in particular at tyrosines 295 and 297, is an important regulator of ZDHHC3 autopalmitoylation. As intermediate reaction products, the increased number of autopalmitoylated ZDHHC3 molecules may derive from an increased rate of palmitate uptake or a reduced rate of acyl moiety delivery to the substrate, suggesting a role for tyrosines 295 and 297 in regulating one of these two steps. Several reports have shown that the interaction between ZDHHCs and their target proteins is dependent on ZDHHC autopalmitoylation (25, 26, 39, 51, 72, 73). In agreement with these data, we observed that the catalytically inactive ZDHHC3/C157S mutant was unable to interact with NCAM, while the ZDHHC3 with five tyrosines mutated had an enhanced ability to interact with NCAM. Presumably, mutation of cytoplasmic tyrosines increased the binding affinity of ZDHHC3 to its substrate in general, since a similar result was observed for another substrate of this PAT-γ2 subunit of the GABA receptor (39) (see Fig. S8 in the supplemental material). Previous work has shown that substrate phosphorylation is a means to regulate the palmitoylation levels of ZDHHC substrate proteins (74, 75). We report here, for the first time, that tyrosine phosphorylation of a PAT is a means to regulate its enzymatic activity.

By analyzing neurite outgrowth in cultured hippocampal neurons, we demonstrated the physiological role of ZDHHC3 tyrosine phosphorylation in neuronal development. By transfection of ZDHHC3wt or its tyrosine mutant in developing neurons, we found that mutation of all the cytoplasmic ZDHHC3 tyrosines caused a significant increase in the total length of the neurites, and this effect was mainly mediated by the increase in the number of neurites. Since NCAM palmitoylation induced by ZDHHC3 (18) was shown to be critical for both NCAM- and FGF2-mediated neurite outgrowth (18, 19), this observation is in agreement with the higher palmitoylating activity of the ZDHHC3 tyrosine mutant toward NCAM180.

Taken together, the results of the present study illustrate the different regulatory roles of tyrosines in the control of ZDHHC3 enzymatic activity, with Y295/297 as a switch off and Y18 as a switch on regulator. This can represent a potential molecular mechanism for the fine-tuning of ZDHHC3 enzymatic activity, depending on the cell type and/or upstream signaling (i.e., FGFR1 or Src). Considering the broad variety of ZDHHC3 substrates and their functional diversity, the regulatory role of tyrosines revealed in this work might not be important just for neuritogenesis. Involvement of ZDHHC3 in the palmitoylation of neurotransmitter receptors (25, 26, 29, 39) assumes the possibility of modulating inhibitory/excitatory synaptic transmission and synaptic plasticity through control of ZDHHC3 tyrosine phosphorylation. Moreover, due to the assumed association of human ZDHHC3 with tumorigenesis (30, 76), regulation of its activity by kinase-dependent tyrosine phosphorylation could be important in controlling cancer progression.

ACKNOWLEDGMENTS

We thank Andrea Barberis for the gift of a vector for expression of the γ2 subunit of the GABA receptor and Masaki Fukata for the gift of vectors for expression of mouse HA-ZDHHC3 and HA-ZDHHC7 and his comments on the manuscript.

This study was supported by the Fondazione San Paolo project "Fat times for neuronal plasticity: mechanisms and significance of extracellular-signal regulated protein palmitoylation" (to A.D.), by the Istituto Italiano di Tecnologia (P.M.-J.L., G.K., and A.D.), by the Deutsche Forschungsgemeinschaft (DFG) through the projects Po732 (to E.P.) and Cluster of Excellence REBIRTH (to E.P.), and by Saint Petersburg State University grant 1.42.1422.2015 (to T.K.).

FUNDING INFORMATION

This work, including the efforts of Alexander Dityatev, was funded by Fondazione San Paolo (Fat times for neuronal plasticity). This work, including the efforts of Evgeni Ponimaskin, was funded by DFG (Po732). This work, including the efforts of Evgeni Ponimaskin, was funded by Cluster of Excellence (Rebirth). This work, including the efforts of Tatiana Kuznetsova, was funded by University of St. Petersburg (1.42.1422.2015).

REFERENCES

1. **Planey SL, Zacharias DA.** 2009. Palmitoyl acyltransferases, their substrates, and novel assays to connect them. Mol Membr Biol **26:**14–31. http://dx.doi.org/10.1080/09687680802646703.

2. **Draper JM, Smith CD.** 2009. Palmitoyl acyltransferase assays and inhibitors. Mol Membr Biol **26:**5–13. http://dx.doi.org/10.1080/09687680802683839.
3. **Greaves J, Chamberlain LH.** 2011. DHHC palmitoyl transferases: substrate interactions and (patho)physiology. Trends Biochem Sci **36:**245–253. http://dx.doi.org/10.1016/j.tibs.2011.01.003.
4. **Korycka J, Lach A, Heger E, Boguslawska DM, Wolny M, Toporkiewicz M, Augoff K, Korzeniewski J, Sikorski AF.** 2012. Human DHHC proteins: a spotlight on the hidden player of palmitoylation. Eur J Cell Biol **91:**107–117. http://dx.doi.org/10.1016/j.ejcb.2011.09.013.
5. **Little EB, Edelman GM, Cunningham BA.** 1998. Palmitoylation of the cytoplasmic domain of the neural cell adhesion molecule N-CAM serves as an anchor to cellular membranes. Cell Adhes Commun **6:**415–430. http://dx.doi.org/10.3109/15419069809109150.
6. **Zeidman R, Jackson CS, Magee AI.** 2009. Protein acyl thioesterases. Mol Membr Biol **26:**32–41. http://dx.doi.org/10.1080/09687680802629329.
7. **Tian L, McClafferty H, Knaus HG, Ruth P, Shipston MJ.** 2012 Distinct acyl protein transferases and thioesterases control surface expression of calcium-activated potassium channels. J Biol Chem **287:**14718–14725. http://dx.doi.org/10.1074/jbc.M111.335547.
8. **Nadolski MJ, Linder ME.** 2007. Protein lipidation. FEBS J **274:**5202–5210. http://dx.doi.org/10.1111/j.1742-4658.2007.06056.x.
9. **Eisenberg S, Laude AJ, Beckett AJ, Mageean CJ, Aran V, Hernandez-Valladares M, Henis YI, Prior IA.** 2013. The role of palmitoylation in regulating Ras localization and function. Biochem Soc Trans **41:**79–83. http://dx.doi.org/10.1042/BST20120268.
10. **Fukata Y, Fukata M.** 2010. Protein palmitoylation in neuronal development and synaptic plasticity. Nat Rev Neurosci **11:**161–175. http://dx.doi.org/10.1038/nrn2788.
11. **Blaskovic S, Blanc M, van der Goot FG.** 2013. What does S-palmitoylation do to membrane proteins? FEBS J **280:**2766–2774. http://dx.doi.org/10.1111/febs.12263.
12. **Sebastiao AM, Colino-Oliveira M, Assaife-Lopes N, Dias RB, Ribeiro JA.** 2013. Lipid rafts, synaptic transmission and plasticity: impact in age-related neurodegenerative diseases. Neuropharmacology **64:**97–107. http://dx.doi.org/10.1016/j.neuropharm.2012.06.053.
13. **Tsui-Pierchala BA, Encinas M, Milbrandt J, Johnson EM, Jr.** 2002. Lipid rafts in neuronal signaling and function. Trends Neurosci **25:**412–417. http://dx.doi.org/10.1016/S0166-2236(02)02215-4.
14. **Guirland C, Zheng JQ.** 2007. Membrane lipid rafts and their role in axon guidance. Adv Exp Med Biol **621:**144–155. http://dx.doi.org/10.1007/978-0-387-76715-4_11.
15. **Kamiguchi H.** 2006. The region-specific activities of lipid rafts during axon growth and guidance. J Neurochem **98:**330–335. http://dx.doi.org/10.1111/j.1471-4159.2006.03888.x.
16. **Ditlevsen DK, Kolkova K.** 2010. Signaling pathways involved in NCAM-induced neurite outgrowth. Adv Exp Med Biol **663:**151–168. http://dx.doi.org/10.1007/978-1-4419-1170-4_10.
17. **Hildebrandt H, Dityatev A.** 2014. With a little help from EphA3 and polysialic acid: ectodomain shedding of NCAM is gaining momentum. J Neurochem **128:**206–209. http://dx.doi.org/10.1111/jnc.12514.
18. **Ponimaskin E, Dityateva G, Ruonala MO, Fukata M, Fukata Y, Kobe F, Wouters FS, Delling M, Bredt DS, Schachner M, Dityatev A.** 2008. Fibroblast growth factor-regulated palmitoylation of the neural cell adhesion molecule determines neuronal morphogenesis. J Neurosci **28:**8897–8907. http://dx.doi.org/10.1523/JNEUROSCI.2171-08.2008.
19. **Niethammer P, Delling M, Sytnyk V, Dityatev A, Fukami K, Schachner M.** 2002. Cosignaling of NCAM via lipid rafts and the FGF receptor is required for neuritogenesis. J Cell Biol **157:**521–532. http://dx.doi.org/10.1083/jcb.200109059.
20. **Kolkova K, Novitskaya V, Pedersen N, Berezin V, Bock E.** 2000. Neural cell adhesion molecule-stimulated neurite outgrowth depends on activation of protein kinase C and the Ras-mitogen-activated protein kinase pathway. J Neurosci **20:**2238–2246.
21. **Francavilla C, Loeffler S, Piccini D, Kren A, Christofori G, Cavallaro U.** 2007. Neural cell adhesion molecule regulates the cellular response to fibroblast growth factor. J Cell Sci **120:**4388–4394. http://dx.doi.org/10.1242/jcs.010744.
22. **Ditlevsen DK, Owczarek S, Berezin V, Bock E.** 2008. Relative role of upstream regulators of Akt, ERK and CREB in NCAM- and FGF2-mediated signaling. Neurochem Int **53:**137–147. http://dx.doi.org/10.1016/j.neuint.2008.06.011.
23. **Gottlieb CD, Zhang S, Linder ME.** 2015. The Cysteine-rich domain of the DHHC3 palmitoyltransferase is palmitoylated and contains tightly bound zinc. J Biol Chem **290:**29259–29269. http://dx.doi.org/10.1074/jbc.M115.691147.
24. **Linder ME, Jennings BC.** 2013. Mechanism and function of DHHC S-acyltransferases. Biochem Soc Trans **41:**29–34. http://dx.doi.org/10.1042/BST20120328.
25. **Hayashi T, Rumbaugh G, Huganir RL.** 2005. Differential regulation of AMPA receptor subunit trafficking by palmitoylation of two distinct sites. Neuron **47:**709–723. http://dx.doi.org/10.1016/j.neuron.2005.06.035.
26. **Hayashi T, Thomas GM, Huganir RL.** 2009. Dual palmitoylation of NR2 subunits regulates NMDA receptor trafficking. Neuron **64:**213–226. http://dx.doi.org/10.1016/j.neuron.2009.08.017.
27. **Gladding CM, Raymond LA.** 2011. Mechanisms underlying NMDA receptor synaptic/extrasynaptic distribution and function. Mol Cell Neurosci **48:**308–320. http://dx.doi.org/10.1016/j.mcn.2011.05.001.
28. **Qiu S, Li XY, Zhuo M.** 2011. Post-translational modification of NMDA receptor GluN2B subunit and its roles in chronic pain and memory. Semin Cell Dev Biol **22:**521–529. http://dx.doi.org/10.1016/j.semcdb.2011.06.003.
29. **Fang C, Deng L, Keller CA, Fukata M, Fukata Y, Chen G, Luscher B.** 2006. GODZ-mediated palmitoylation of GABA(A) receptors is required for normal assembly and function of GABAergic inhibitory synapses. J Neurosci **26:**12758–12768. http://dx.doi.org/10.1523/JNEUROSCI.4214-06.2006.
30. **Sharma C, Rabinovitz I, Hemler ME.** 2012. Palmitoylation by DHHC3 is critical for the function, expression, and stability of integrin alpha6beta4. Cell Mol Life Sci **69:**2233–2244. http://dx.doi.org/10.1007/s00018-012-0924-6.
31. **Deyts C, Vetrivel KS, Das S, Shepherd YM, Dupre DJ, Thinakaran G, Parent AT.** 2012. Novel GalphaS-protein signaling associated with membrane-tethered amyloid precursor protein intracellular domain. J Neurosci **32:**1714–1729. http://dx.doi.org/10.1523/JNEUROSCI.5433-11.2012.
32. **Neves SR, Ram PT, Iyengar R.** 2002. G protein pathways. Science **296:**1636–1639. http://dx.doi.org/10.1126/science.1071550.
33. **Tsutsumi R, Fukata Y, Noritake J, Iwanaga T, Perez F, Fukata M.** 2009. Identification of G protein alpha subunit-palmitoylating enzyme. Mol Cell Biol **29:**435–447. http://dx.doi.org/10.1128/MCB.01144-08.
34. **Levy AD, Devignot V, Fukata Y, Fukata M, Sobel A, Chauvin S.** 2011. Subcellular Golgi localization of stathmin family proteins is promoted by a specific set of DHHC palmitoyl transferases. Mol Biol Cell **22:**1930–1942. http://dx.doi.org/10.1091/mbc.E10-10-0824.
35. **Jennings BC, Linder ME.** 2012. DHHC protein S-acyltransferases use similar ping-pong kinetic mechanisms but display different acyl-CoA specificities. J Biol Chem **287:**7236–7245. http://dx.doi.org/10.1074/jbc.M111.337246.
36. **Lu D, Sun HQ, Wang H, Barylko B, Fukata Y, Fukata M, Albanesi JP, Yin HL.** 2012. Phosphatidylinositol 4-kinase IIalpha is palmitoylated by Golgi-localized palmitoyltransferases in cholesterol-dependent manner. J Biol Chem **287:**21856–21865. http://dx.doi.org/10.1074/jbc.M112.348094.
37. **Oku S, Takahashi N, Fukata Y, Fukata M.** 2013. In silico screening for palmitoyl substrates reveals a role for DHHC1/3/10 (zDHHC1/3/11)-mediated neurochondrin palmitoylation in its targeting to Rab5-positive endosomes. J Biol Chem **288:**19816–19829. http://dx.doi.org/10.1074/jbc.M112.431676.
38. **Lievens PM, Liboi E.** 2003. The thanatophoric dysplasia type II mutation hampers complete maturation of fibroblast growth factor receptor 3 (FGFR3), which activates signal transducer and activator of transcription 1 (STAT1) from the endoplasmic reticulum. J Biol Chem **278:**17344–17349. http://dx.doi.org/10.1074/jbc.M212710200.
39. **Keller CA, Yuan X, Panzanelli P, Martin ML, Alldred M, Sassoe-Pognetto M, Luscher B.** 2004. The gamma2 subunit of GABA(A) receptors is a substrate for palmitoylation by GODZ. J Neurosci **24:**5881–5891. http://dx.doi.org/10.1523/JNEUROSCI.1037-04.2004.
40. **Wirth A, Chen-Wacker C, Wu YW, Gorinski N, Filippov MA, Pandey G, Ponimaskin E.** 2013. Dual lipidation of the brain-specific Cdc42 isoform regulates its functional properties. Biochem J **456:**311–322. http://dx.doi.org/10.1042/BJ20130788.
41. **Yap MC, Kostiuk MA, Martin DD, Perinpanayagam MA, Hak PG, Siddam A, Majjigapu JR, Rajaiah G, Keller BO, Prescher JA, Wu P, Bertozzi CR, Falck JR, Berthiaume LG.** 2010. Rapid and selective detection of fatty acylated proteins using omega-alkynyl-fatty acids and click chemistry. J Lipid Res **51:**1566–1580. http://dx.doi.org/10.1194/jlr.D002790.
42. **Hang HC, Wilson JP, Charron G.** 2011. Bioorthogonal chemical report-

ers for analyzing protein lipidation and lipid trafficking. Acc Chem Res **44:**699–708. http://dx.doi.org/10.1021/ar200063v.
43. **Martin, BR.** 2013. Nonradioactive analysis of dynamic protein palmitoylation. Curr Protoc Protein Sci Chapter 73:Unit 14.15. http://dx.doi.org/10.1002/0471140864.ps1415s73.
44. **Storck EM, Serwa RA, Tate EW.** 2013. Chemical proteomics: a powerful tool for exploring protein lipidation. Biochem Soc Trans **41:**56–61. http://dx.doi.org/10.1042/BST20120283.
45. **Gao X, Hannoush RN.** 2014. Single-cell in situ imaging of palmitoylation in fatty-acylated proteins. Nat Protoc **9:**2607–2623. http://dx.doi.org/10.1038/nprot.2014.179.
46. **Dityatev A, Bruckner G, Dityateva G, Grosche J, Kleene R, Schachner M.** 2007. Activity-dependent formation and functions of chondroitin sulfate-rich extracellular matrix of perineuronal nets. Dev Neurobiol **67:**570–588. http://dx.doi.org/10.1002/dneu.20361.
47. **Dityateva G, Hammond M, Thiel C, Ruonala MO, Delling M, Siebenkotten G, Nix M, Dityatev A.** 2003. Rapid and efficient electroporation-based gene transfer into primary dissociated neurons. J Neurosci Methods **130:**65–73. http://dx.doi.org/10.1016/S0165-0270(03)00202-4.
48. **Degasperi A, Birtwistle MR, Volinsky N, Rauch J, Kolch W, Kholodenko BN.** 2014. Evaluating strategies to normalise biological replicates of Western blot data. PLoS One **9:**e87293. http://dx.doi.org/10.1371/journal.pone.0087293.
49. **Kiselyov VV, Skladchikova G, Hinsby AM, Jensen PH, Kulahin N, Soroka V, Pedersen N, Tsetlin V, Poulsen FM, Berezin V, Bock E.** 2003. Structural basis for a direct interaction between FGFR1 and NCAM and evidence for a regulatory role of ATP. Structure **11:**691–701. http://dx.doi.org/10.1016/S0969-2126(03)00096-0.
50. **Dalva MB.** 2009. Neuronal activity moves protein palmitoylation into the synapse. J Cell Biol **186:**7–9. http://dx.doi.org/10.1083/jcb.200906101.
51. **Noritake J, Fukata Y, Iwanaga T, Hosomi N, Tsutsumi R, Matsuda N, Tani H, Iwanari H, Mochizuki Y, Kodama T, Matsuura Y, Bredt DS, Hamakubo T, Fukata M.** 2009. Mobile DHHC palmitoylating enzyme mediates activity-sensitive synaptic targeting of PSD-95. J Cell Biol **186:**147–160. http://dx.doi.org/10.1083/jcb.200903101.
52. **Fukata Y, Dimitrov A, Boncompain G, Vielemeyer O, Perez F, Fukata M.** 2013. Local palmitoylation cycles define activity-regulated postsynaptic subdomains. J Cell Biol **202:**145–161. http://dx.doi.org/10.1083/jcb.201302071.
53. **Lai J, Linder ME.** 2013. Oligomerization of DHHC protein S-acyltransferases. J Biol Chem **288:**22862–22870. http://dx.doi.org/10.1074/jbc.M113.458794.
54. **Lakkaraju AK, Abrami L, Lemmin T, Blaskovic S, Kunz B, Kihara A, Dal Peraro M, van der Goot FG.** 2012. Palmitoylated calnexin is a key component of the ribosome-translocon complex. EMBO J **31:**1823–1835. http://dx.doi.org/10.1038/emboj.2012.15.
55. **Zhan X, Plourde C, Hu X, Friesel R, Maciag T.** 1994. Association of fibroblast growth factor receptor-1 with c-Src correlates with association between c-Src and cortactin. J Biol Chem **269:**20221–20224.
56. **Li W, Lee J, Vikis HG, Lee SH, Liu G, Aurandt J, Shen TL, Fearon ER, Guan JL, Han M, Rao Y, Hong K, Guan KL.** 2004. Activation of FAK and Src are receptor-proximal events required for netrin signaling. Nat Neurosci **7:**1213–1221. http://dx.doi.org/10.1038/nn1329.
57. **Li X, Brunton VG, Burgar HR, Wheldon LM, Heath JK.** 2004. FRS2-dependent SRC activation is required for fibroblast growth factor receptor-induced phosphorylation of Sprouty and suppression of ERK activity. J Cell Sci **117:**6007–6017. http://dx.doi.org/10.1242/jcs.01519.
58. **Yu H, Chen JK, Feng S, Dalgarno DC, Brauer AW, Schreiber SL.** 1994. Structural basis for the binding of proline-rich peptides to SH3 domains. Cell **76:**933–945. http://dx.doi.org/10.1016/0092-8674(94)90367-0.
59. **Auciello G, Cunningham DL, Tatar T, Heath JK, Rappoport JZ.** 2013. Regulation of fibroblast growth factor receptor signalling and trafficking by Src and Eps8. J Cell Sci **126:**613–624. http://dx.doi.org/10.1242/jcs.116228.
60. **Sandilands E, Akbarzadeh S, Vecchione A, McEwan DG, Frame MC, Heath JK.** 2007. Src kinase modulates the activation, transport and signalling dynamics of fibroblast growth factor receptors. EMBO Rep **8:**1162–1169. http://dx.doi.org/10.1038/sj.embor.7401097.
61. **Sytnyk V, Leshchyns'ka I, Delling M, Dityateva G, Dityatev A, Schachner M.** 2002. Neural cell adhesion molecule promotes accumulation of TGN organelles at sites of neuron-to-neuron contacts. J Cell Biol **159:**649–661. http://dx.doi.org/10.1083/jcb.200205098.
62. **Hines RM, Kang R, Goytain A, Quamme GA.** 2010. Golgi-specific DHHC zinc finger protein GODZ mediates membrane Ca2+ transport. J Biol Chem **285:**4621–4628. http://dx.doi.org/10.1074/jbc.M109.069849.
63. **Fukata Y, Iwanaga T, Fukata M.** 2006. Systematic screening for palmitoyl transferase activity of the DHHC protein family in mammalian cells. Methods **40:**177–182. http://dx.doi.org/10.1016/j.ymeth.2006.05.015.
64. **LaVallee TM, Prudovsky IA, McMahon GA, Hu X, Maciag T.** 1998. Activation of the MAP kinase pathway by FGF-1 correlates with cell proliferation induction while activation of the Src pathway correlates with migration. J Cell Biol **141:**1647–1658. http://dx.doi.org/10.1083/jcb.141.7.1647.
65. **Boilly B, Vercoutter-Edouart AS, Hondermarck H, Nurcombe V, Le Bourhis X.** 2000. FGF signals for cell proliferation and migration through different pathways. Cytokine Growth Factor Rev **11:**295–302. http://dx.doi.org/10.1016/S1359-6101(00)00014-9.
66. **Rodier JM, Valles AM, Denoyelle M, Thiery JP, Boyer B.** 1995. pp60c-src is a positive regulator of growth factor-induced cell scattering in a rat bladder carcinoma cell line. J Cell Biol **131:**761–773. http://dx.doi.org/10.1083/jcb.131.3.761.
67. **Bonneton C, Sibarita JB, Thiery JP.** 1999. Relationship between cell migration and cell cycle during the initiation of epithelial to fibroblastoid transition. Cell Motil Cytoskeleton **43:**288–295.
68. **Liu J, Huang C, Zhan X.** 1999. Src is required for cell migration and shape changes induced by fibroblast growth factor 1. Oncogene **18:**6700–6706. http://dx.doi.org/10.1038/sj.onc.1203050.
69. **Lobo S, Greentree WK, Linder ME, Deschenes RJ.** 2002. Identification of a Ras palmitoyltransferase in Saccharomyces cerevisiae. J Biol Chem **277:**41268–41273. http://dx.doi.org/10.1074/jbc.M206573200.
70. **Roth AF, Feng Y, Chen L, Davis NG.** 2002. The yeast DHHC cysteine-rich domain protein Akr1p is a palmitoyl transferase. J Cell Biol **159:**23–28. http://dx.doi.org/10.1083/jcb.200206120.
71. **Mitchell DA, Mitchell G, Ling Y, Budde C, Deschenes RJ.** 2010. Mutational analysis of Saccharomyces cerevisiae Erf2 reveals a two-step reaction mechanism for protein palmitoylation by DHHC enzymes. J Biol Chem **285:**38104–38114. http://dx.doi.org/10.1074/jbc.M110.169102.
72. **Fernandez-Hernando C, Fukata M, Bernatchez PN, Fukata Y, Lin MI, Bredt DS, Sessa WC.** 2006. Identification of Golgi-localized acyl transferases that palmitoylate and regulate endothelial nitric oxide synthase. J Cell Biol **174:**369–377. http://dx.doi.org/10.1083/jcb.200601051.
73. **Huang K, Sanders SS, Kang R, Carroll JB, Sutton L, Wan J, Singaraja R, Young FB, Liu L, El-Husseini A, Davis NG, Hayden MR.** 2011. Wild-type HTT modulates the enzymatic activity of the neuronal palmitoyl transferase HIP14. Hum Mol Genet **20:**3356–3365. http://dx.doi.org/10.1093/hmg/ddr242.
74. **Charych EI, Jiang LX, Lo F, Sullivan K, Brandon NJ.** 2010 Interplay of palmitoylation and phosphorylation in the trafficking and localization of phosphodiesterase 10A: implications for the treatment of schizophrenia. J Neurosci **30:**9027–9037. http://dx.doi.org/10.1523/JNEUROSCI.1635-10.2010.
75. **Salaun C, Greaves J, Chamberlain LH.** 2010. The intracellular dynamic of protein palmitoylation. J Cell Biol **191:**1229–1238. http://dx.doi.org/10.1083/jcb.201008160.
76. **Oh Y, Jeon YJ, Hong GS, Kim I, Woo HN, Jung YK.** 2012. Regulation in the targeting of TRAIL receptor 1 to cell surface via GODZ for TRAIL sensitivity in tumor cells. Cell Death Differ **19:**1196–1207. http://dx.doi.org/10.1038/cdd.2011.209.